DROP-IT

DELIVERABLE 4.1

Inkjet-printed RGB LEDs based on BLFP (benchmark) with EQE>14% for green

Due date of deliverable: 2021/10/31

Actual submission date: 2022/07/08

Deliverable number:	D4.1
Due date:	31.10.2021
Nature[1]:	R
Dissemination Level[1]:	PU
Work Package:	WP4
Lead Beneficiary:	UJI
Contributing Beneficiaries:	UB

[1] **Nature:** R = Report, P = Prototype, D = Demonstrator, O = Other
Dissemination level PU = Public PP = Restricted to other programme participants (including the Commission Services) RE = Restricted to a group specified by the consortium (including the Commission Services) CO = Confidential, only for members of the consortium (including the Commission Services) Restraint UE = Classified with the classification level "Restraint UE" according to Commission Deci-sion 2001/844 and amendments Confidential UE = Classified with the mention of the classification level "Confidential UE" according to Commission Decision 2001/844 and amendments Secret UE = Classified with the mention of the classification level "Secret UE" according to Commis-sion Decision 2001/844 and amendments

This project has received funding from the European Union's Horizon 2020 research and innovation programme under **Grant Agreement No. 862656**.

DOCUMENT HISTORY

Version	***Date***	***Reason of change***
1	2021/11/29	UB contribution
2	2021/11/29	UJI contribution
3	2022/06/30	UB contribution
4	2022/07/01 – 2022/07/07	UJI contribution and revision by the partners

This project has received funding from the European Union's Horizon 2020 research and innovation programme under **Grant Agreement No. 862656**.

Table of Content

1 INTRODUCTION 5

2 DESCRIPTION OF WORK & MAIN ACHIEVEMENTS 6

2.1 INKJET PRINTING 6

2.1.1 Sn-based based perovskites 6

2.1.1.1 Preparation of ink based on $FASnBr_3$, $MASnBr_3$ from precursors (from SAULE) for yellow and red emission, respectively as the B-LFP. 6

2.1.1.2 Preparation of ink based on TEA_2SnI_4 (from ETHZ) and PEA_2SnI_4 for red emission 7

2.1.1.1 Preparation of $(OLAm)_2SnBr_4$ 2D perovskites for orange emission 7

2.1.1.2 Sn(II) doped CsBr materials: 8

2.1.1.3 Bi^{3+}-doped Cs_2SnCl_6 Nanocrystals: 9

2.1.2 $Cs_3Cu_2I_5$ perovskites 9

2.1.2.1 Preparation of ink based on $Cs_3Cu_2I_5$ from precursors (from ETHZ) for blue emission. 9

2.1.2.2 Preparation of ink based on $Cs_3Cu_2I_5$ from NCs (from NCs) for blue emission. 10

2.1.3 $Rb_3InCl_6:Sb^{3+}$ from precursors in DMSO or MFA 11

2.1.3.1 Preparation of ink based on $Rb_3InCl_6:Sb^{3+}$ from precursors (from ETHZ) for green emission. 11

2.1.4 $Cs_2AgNaInCl_6:Bi^{3+}$ pseudo-perovskites 13

2.1.4.1 Preparation of ink based on $Cs_2AgNaInCl_6:Bi^{3+}$ from NCs (from ETHZ) for white emission. 13

2.2 INKJET PRINTING CONDITIONS 15

2.2.1 Devices 15

2.3 MATERIAL AND PRELIMINARY DEVICE CHARACTERIZATION 16

3 RESULTS 17

3.1 STRUCTURAL, OPTICAL AND MORPHOLOGICAL PROPERTIES OF THE INKJET PRINTED BENCHMARK Sn^{2+}-BASED THIN FILMS FOR RED AND YELLOW EMISSION. 17

3.1.1 $FASnBr_3$, $MASnBr_3$ from precursors (from SAULE) 17

3.2 STRUCTURAL, OPTICAL AND MORPHOLOGICAL PROPERTIES OF THE INKJET PRINTED $Cs_3Cu_2I_5$ PSEUDO-PEROVSKITES THIN FILMS FOR BLUE EMISSION 21

3.2.1 $Cs_3Cu_2I_5$ from precursor (from ETHZ) 21

3.2.2 $Cs_3Cu_2I_5$ from NCs (from UJI) 24

3.3 STRUCTURAL, OPTICAL AND MORPHOLOGICAL PROPERTIES OF THE INKJET PRINTED $Cs_2AgNaInCl_6:Bi^{3+}$ PSEUDO-PEROVSKITES THIN FILMS FOR WHITE EMISSION 25

3.3.1 $Cs_2AgNaInCl_6:Bi^{3+}$ from NCs (from ETHZ) 25

3.4 STRUCTURAL, OPTICAL AND MORPHOLOGICAL PROPERTIES OF THE INKJET PRINTED 2D PEROVSKITES TEA_2SnI_4 AND PEA_2SnI_4 THIN FILMS FOR RED EMISSION 27

3.4.1 TEA_2SnI_4 from precursor (ETHZ) 27

This project has received funding from the European Union's Horizon 2020 research and innovation programme under **Grant Agreement No. 862656**.

3.4.2 PEA_2SnI_4 from precursor (UJI) 30

3.5 CHARACTERIZATION OF RED EMITTING PEROVSKITE PEA_2SnI_4 LEDS WITH ADDITIVES SnF_2 AND $NaBH_4$ 32

4 DEVIATIONS FROM THE WORKPLAN 36

5 CONCLUSIONS & FUTURE DIRECTIONS 36

This project has received funding from the European Union's Horizon 2020 research and innovation programme under **Grant Agreement No. 862656**.

1 Introduction

Fabrication and optimization of single-color LEDs (p-i-n configuration) based on B-LFPs (Sn^{2+}-cation with appropriate content of Cl-Br-I anion to define the color) deposited by inkjet printing on flexible substrates in order to obtain EQE>14% for green.

Purpose of the report

From Task 4.1 we arrived at the most suitable device structures and architectures, where the validated transport layers are tested with the selected promising new generation lead-free perovskite (G-LFP). The new interfaces were studied in terms of bandgap, electro-optical properties, stability and processability.

The full implementation by inkjet printing onto flexible substrate of single-color LED device based on G-LFP is the main objective of this report. Several inkjet-printed B-LFP thin films ($FASnBr_3$, $MASnBr_3$, $MAFASnBr_3$, $MASnI_3$) were previously tested, as benchmark in terms of efficiency and stability, D2.5, but none of them showed promising results after inkjet printing the thin active layers, due to low PL emission, PLQY values below 1%. Consequently, the main efforts were focused on the G-LFP performance. The single LED devices based on the G-LFPs selected and evaluated in WP1 with appropriate bandgap and formulated for inkjet in WP2 and interfacing with appropriate charge transport layers in Task 4.1 are presented with the developed structural, chemical, optical and optoelectronic (LED efficiency and electrical parameters) characterization.

Tin-based perovskite nanomaterials which exhibit narrower bandgap and comparable photophysical properties to its lead analogues, is one of the most forward-looking lead-free perovskite semiconductor candidates to replace lead halide perovskites in lighting applications.

Sn^{2+} is the most obvious candidate to substitute Pb^{2+} because of their similar ionic radius (Pb: 1.49 Å, Sn: 1.35 Å) and outer shell electronic configuration (ns^2), which enables crystallizing a perovskite structure with the formula $ASnX_3$ isostructural to the lead halide-based counterparts.

However, Sn^{2+} is prone to be oxidized and forming its tetravalent state Sn^{4+}, which leads to a high defect density and generates trap states, thereby lowering the radiative recombination. Therefore, the low stability of tin perovskite hinders the development toward potential optoelectronic application.

Among the possible emissive perovskites with the formula $ASnX_3$, we tested $FASnBr_3$ and $MASnBr_3$ with expected emission in yellow and red range, respectively. Notwithstanding inkjet-printed pinhole-free uniform layers, low PL emissions were measured to ensure promising devices.

In parallel to the benchmark Sn^{2+}-based materials, other efforts were focused on a current promising Pb-free metal halide, 0D $Cs_3Cu_2I_5$ possessing high PLQY (~87% blue emission), produced from both the molecular precursor and colloidal NCs synthesis approaches. At the present scenario of the project, this emerging copper halide materials shown excellent stability, without any encapsulation and protection, also demonstrated remarkable stability against oxygen and water degradation after a 35-days storage in air ambient.

Recently, all-inorganic lead-free 0D perovskite Cs_4SnBr_6 has been reported with the PLQY of 15.5%, while the Sn^{2+} ion is extremely unstable and easily oxidized to Sn^{4+}. Afterwards, relatively stable all-inorganic lead-free 0D perovskites based on higher-valence octahedral central cations (Hf^{4+}, Zr^{4+}, Ti^{4+}, Bi^{3+}, and In^{3+}) have been widely studied. As mentioned earlier, the reported PLQY of all-inorganic 0D cesium copper(I) iodide with tetrahedral structure is about 90%. Zero-dimensional (0D) lead-free perovskites have unique structures and optoelectronic properties as showed also by the

Sb^{3+}-doped all inorganic, lead-free, 0D Rb_2InCl_6 perovskite which exhibits greatly enhanced green emission with a PLQY widening from <2% to 85–95% through doping the $Rb_2InCl_5(H_2O)$ with Sb^{3+}.[1,2] The main drawback of 0D materials for LEDs devices fabrication is the self-trapped excitonic (STE) emission which makes very challenging to observe EL phenomena.

In view of all the reported materials, in recent years, 2D halide perovskites have become a striking research spotlight. It is noteworthy that low-dimensional Sn^{2+}-based halide perovskites exhibit remarkably enhanced air stability in comparison with their 3D counterparts. In this work, the stability and emission properties of single-layer 2D tin perovskite nanoplates with chemical formula TEA_2SnI_4 (TEA = 2-thiophene-ethylammonium) and PEA_2SnI_4 (PEA = phenethylammonium) both with strong red emission are reported.

Among all the tested devices, the inkjet-printed PEA_2SnI_4-based light-emitting diode (LED) is the one which exhibits, in ambient conditions after encapsulation, a maximum external quantum efficiency (EQE) of 1% with an average of 0.7% and a brightness of 30 cd m^{-2}, which are comparable to that of the control devices obtained by spin coating and the first in literature. Moreover, a lifetime test shows an operating half-life exceeding 3 hours at an initial brightness of 10 cd/m^2.

2 Description of work & main achievements

2.1 Inkjet printing

2.1.1 Sn-based based perovskites

Most of the Sn^{2+}-based perovskite studies focused on the $FASnI_3$ and $MASnI_3$ material, having a band-gap value around 1.2–1.3 eV and a tetragonal crystal structure. Less extensive investigations are available regarding other halogens in Sn-based systems like $FASnBr_3$ and $MASnBr_3$. Ferrara et al. investigated the synthesis, crystal structure, and optical properties of the $FA_{1-x}MA_xSnBr_3$ system, reporting for the first time of $FASnBr_3$ material and the formation of a solid solution between the two end members, which possess a cubic symmetry with lattice parameter and cell volume obeying Vegard's law.[3]

Palazon et al. demonstrated a tunable wide-bandgap monohalide perovskite, showing very promising $FASnBr_3$ and $MASnBr_3$ materials with bandgaps in the range of 1.7-1.9 eV.[4]

Following the list of tested Sn^{+2}-based materials.

2.1.1.1 Preparation of ink based on $FASnBr_3$, $MASnBr_3$ from precursors (from SAULE) for yellow and red emission, respectively as the B-LFP.

In the previous work presented in D2.3 was described the main characteristic of the ink formulation for the family of Sn^{2+}-based inks from precursors.
The precursor inks were prepared using commercially available precursors (DMSO and DMF) inside a nitrogen filled glovebox with well controlled oxygen and humidity levels below 1 ppm. The recipe for the $FASnI_3$ composition was adopted from Jiang et al.[5]and modified to meet the inkjet printing

requirements. In particular, it was important to reduce the concentration of the precursor ink and a solvent ratio (DMSO:DMF, 4:1) to enable inkjet printing and achieve a submicron thick film.
For the other inks the work of Ferrara *et al.* [3] and Mathies *et al.* [6,7] were considered to reach the best solutions. The expected colours for the films were obtained: yellow ($FASnBr_3$), red ($MASnBr_3$) and dark (for the $MASnI_3$ and $FASnI_3$).

i) $MASnBr_3$ ($MABr+SnBr_2$)
ii) $FASnBr_3$ ($FABr+SnBr_2$)

1. Solution $MASnBr_3$ (c= e.g., 1mol/L) V=2ml
2. Solution $FASnBr_3$ (c= e.g., 1mol/L) V=2ml

2.1.1.2 Preparation of ink based on TEA_2SnI_4 (from ETHZ) and PEA_2SnI_4 for red emission

Several research moved to improve the emission quantum efficiency of nanoscale 2D layered tin iodide perovskites through fine-tuning the electronic properties of organic ammonium salts. Under optimized conditions, a PLQY up to 21% was accomplished for the thienylethylammonium tin iodide perovskite (TEA_2SnI_4).[8]

Another work demonstrates that ammonium thiocyanate (NH_4SCN) is the most effective additive in enhancing the stability and photoluminescence quantum yield of 2D TEA_2SnI_4 (23 ± 3%).[9]

Bearing in mind the promising results from literature, as a possible alternative to the presented 3D Sn^{2+}-based perovskite family, also is implemented the production of 2D structured materials as well. We received from the ETHZ partner the precursor solution for TEA_2SnI_4 which holds the record for PLQY in this family of compounds (23%)[9] and from UJI partner the precursor solution for PEA_2SnI_4. Both ink solutions are based on a concentration of DMSO with a molar ratio of 0.67 and 0.25, respectively. In the case of TEA_2SnI_4 the purified SnI_2 was employed.
In the case of TEA_2SnI_4 two possible additive are implemented, SnF_2 and $NaBH_4$.

2.1.1.1 Preparation of $(OLAm)_2SnBr_4$ 2D perovskites for orange emission

In this section, we have performed the synthesis of 2D Ruddlesden−Popper type oleylammonium tin bromide ($(C_{18}H_{35}NH_3)_2SnBr_4$) by a modified hot-injection method, by combining main precursors conventional oleic acid/oleylamine and $SnBr_2$-trioctylphosphine. The existence of $OLAm^+$ cations into the perovskite avoid the electronic band formation between $[SnBr_6]^{4-}$ octahedra composing the material structure, which induces the generation of orange-light emission with a strong Stokes-shift. The emissive property of the perovskite is associated to existence of the self-trapped energy levels from the above $[SnBr_6]^{4-}$-octahedra, providing high optical performances, mainly photoluminescence quantum yield (PLQY ~88%)[10]. According with the experience in preparation of perovskite nanoparticles, we have synthesized orange-emitting $(OLAm)_2SnBr_4$ with 100% PLQY, with an absorption edge below 350 nm, emission feature of 625 nm (high Stokes-shift ~300 nm) and full width and half maximum of 145 nm (Figure 1).

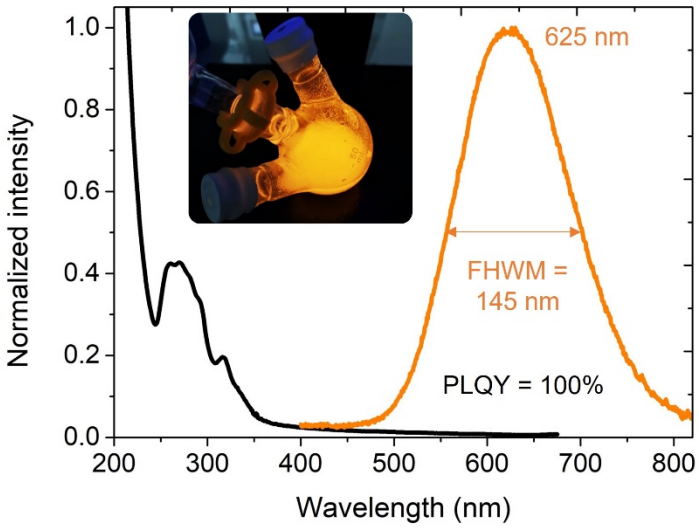

Figure 1. Absorption and emission spectra of $(OLAm)_2SnBr_4$ dispersed in octane. Inset of Figure xxx shows the typical orange-emitting features of the as-prepared material.

2.1.1.2 Sn(II) doped CsBr materials:

Sn(II) doped CsBr absorbs visible light near 430 nm, and emits broad orange light centred near 600 nm with the PLQY ~21.5 % (Figure 2). A small percentage of interstitial doping of Sn(II) in CsBr lattice shows such excellent optical feature. Sn(II) doped CsBr was prepared using a continuous flow reactor following antisolvent mediated recrystallization method. In a typical method, CsBr and $SnBr_2$ were dissolved in DMF, and toluene was used as the antisolvent to recrystallize the product. The final material was redispersed in toluene and used as an ink for the further procedures.[11])

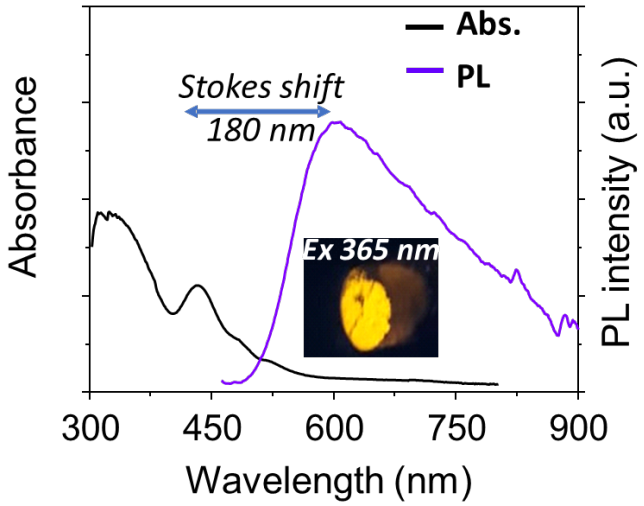

Figure 2. Absorbance (black line) and photoluminescence (indigo line) of Sn(II) doped CsBr materials. Inset shows illuminated material under 365 nm UV lamp.

Sn^{4+}-based Materials:

2.1.1.3 Bi^{3+}-doped Cs_2SnCl_6 Nanocrystals:

Bi^{3+} doped Cs_2SnCl_6 nanocrystals were prepared followed by wet-chemical approach. In a typical method, Cs-acetate, Sn(II)-acetate and Bi(III)-acetate were reacted with oleic acid to prepare metal oleates. In the second step, HCl was treated with the metal oleates, followed by the washing with acetone. The as-prepared nanocrystals were collected by centrifugation. In the final step, the as-prepared nanocrystals were treated with oleylamine, and dispersed in dodecane for the use as an ink. This material absorbs UV light near 340 nm, and emits blue light near 450 nm (PLQY ~26.5%). The optical characterizations are provided in Figure 3.

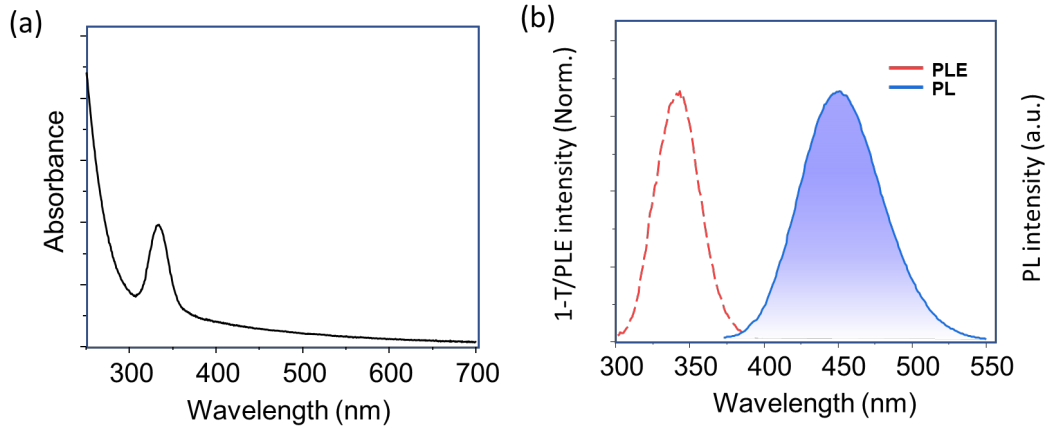

Figure 3. (a) Absorbance and (b) PLE (red dashed) and PL (blue line) spectra of Bi^{3+} doped Cs_2SnCl_6 nanocrystals.

2.1.2 $Cs_3Cu_2I_5$ perovskites

Ternary copper halide compounds with monovalent Cu^+ has recently attracted great research interest due to their optoelectronic performances. Han *et al.* first reported the colloidal synthesis of low dimensional cesium copper halide NCs (including 0D $Cs_3Cu_2I_5$ and 1D $CsCu_2I_3$) and demonstrated that the reaction temperature is crucial for the morphological structure. *Angewandte Chemie International Edition, vol. 58, no. 45, pp. 16087–16091, 2019.*

The 0D $Cs_3Cu_2I_5$ NCs showed a strong blue emission peaked at 441 nm with a PLQY up to 67%, while 1D $CsCu_2I_3$ NRs exhibited a weak yellow emission centered at 553 nm with a PLQY of 5%. *Advanced Materials, vol. 30, no. 43, article 1804547, 2018.*

Accordingly, Shi *et al.* achieved an obvious enhancement in the PLQY of $Cs_3Cu_2I_5$ NCs up to ~87% with a large exciton binding energy (138.4 meV), thus paving the way for very promising optoelectronics devices[12]

2.1.2.1 Preparation of ink based on $Cs_3Cu_2I_5$ from precursors (from ETHZ) for blue emission.

We received the $Cs_3Cu_2I_5$ from the molecular precursor solution in DMSO (0.47 M) with high concentration. We can obtain quite uniform printed layers with bright blue emission. For registering the photoluminescence signal, this material must be excited at 260-320 nm.

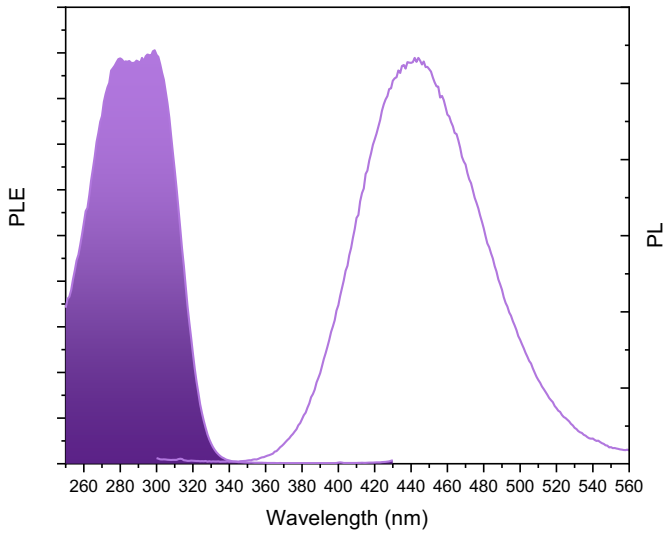

Figure 4. Optical properties of $Cs_3Cu_2I_5$ films

2.1.2.2 Preparation of ink based on $Cs_3Cu_2I_5$ from NCs (from NCs) for blue emission.

Cs_3CuI_5 nanocrystals were synthesized following a hot-injection synthesis approach. In a typical method, Cs-oleate was prepared by reacting Cs_2CO_3 and oleic acid in 1-octadecene at 130 °C. On the other hand, CuI precursor was treated with oleylamine and oleic acid in 1-octadecene in order to dissolve. This treatment was carried out at 120 °C. After the complete dissolution of CuI precursor, the temperature was cooled down to 60 °C, and Cs-oleate precursor was injected followed by the ice-quenching. The as-prepared nanocrystals were collected by centrifugation of the reaction product. The nanocrystals were harvested in hexane. $Cs_3Cu_2I_5$ nanocrystals has an absorption near 280 nm, and it has a direct band gap. It emits blue light near 450 nm (PLQY ~100%) originated from the self-trapped excitons (Figure 5).

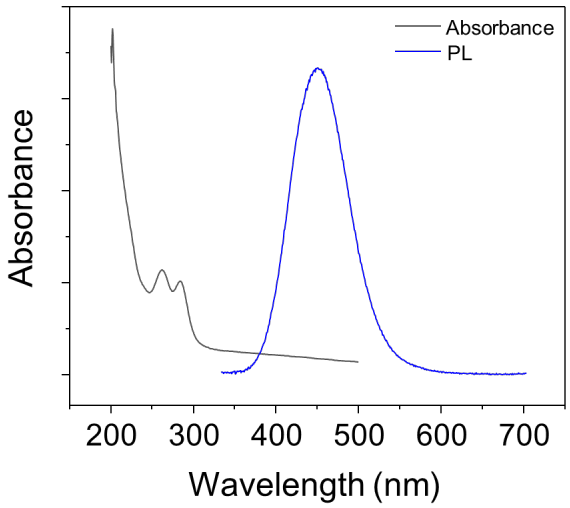

Figure 5. Absorbance (black line) and PL (blue line) of $Cs_3Cu_2I_5$ nanocrystals prepared using hot-injection synthesis approach.

2.1.3 $Rb_3InCl_6:Sb^{3+}$ from precursors in DMSO or MFA

2.1.3.1 Preparation of ink based on $Rb_3InCl_6:Sb^{3+}$ from precursors (from ETHZ) for green emission.

For the **green-emitting material** the only one LFP up to date is **Rb_3InCl_6 doped with Sb^{3+}.** This material is reported to exhibit cyan-green broadband emission upon excitation at 325-345 nm exhibiting reasonable PL QY (about 20-40% in some reports) in form of NCs.

For inkjet printing have been tested NCs in dodecane and precursors solutions in polar solvents (DMSO) and N-methylformamide (MFA).

1. Solution in MFA can be prepared with concentration up to 0.2 M, quite bright (PL QY ~85%) and nearly phase-pure $Rb_3InCl_6:Sb^{3+}$ crystals can be obtained. However, this solution has tendency to form crystals, not uniform films.

2. Solution in DMSO can be prepared with concentration up to 0.125 M. Reasonably uniform films from DMSO can be reached, however PLQY is notably low, 26 %.

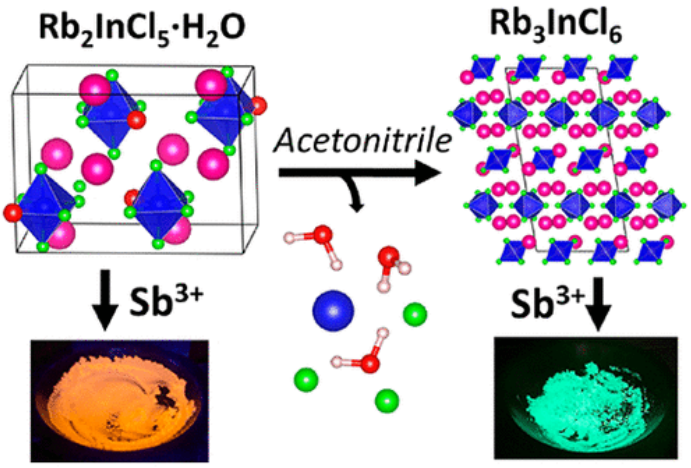

Bulk:
Inorg. Chem. 2020, 59, 14478−14485
Angew. Chem. Int. Ed. 2020, 59, 12709−12713
Adv. Optical Mater. 2021, 9, 2002267

NCs: ACS Energy Lett. 2021, 6, 6, 2283−2292

compound	PLE max, nm	PL max, nm	PL QY, %
Rb_3InCl_6:Sb	345±35 325±25	520±80 497±70	95

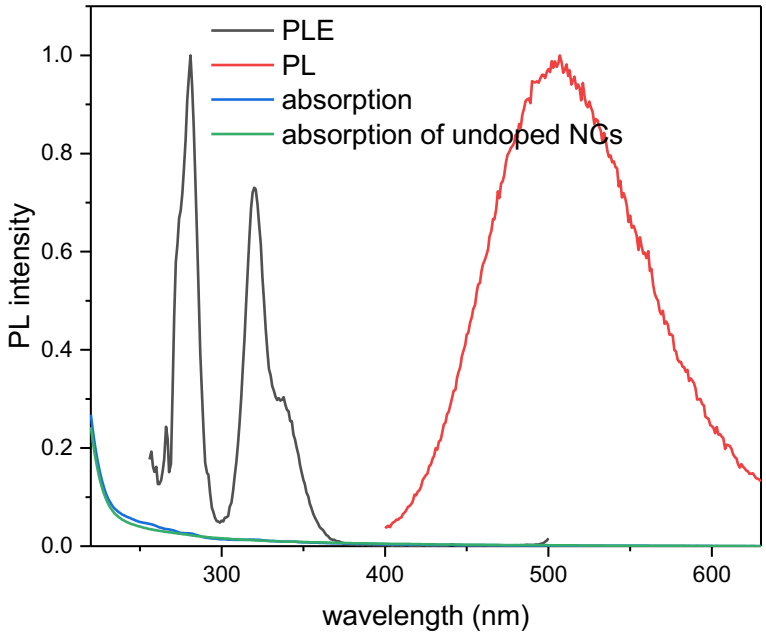

Figure 6. Absorbance (blue and green lines) and PLE (dark line) and PL (red line) of Rb_3InCl_6 nanocrystals.

2.1.4 $Cs_2AgNaInCl_6:Bi^{3+}$ pseudo-perovskites

2.1.4.1 Preparation of ink based on $Cs_2AgNaInCl_6:Bi^{3+}$ from NCs (from ETHZ) for white emission.

For the $Cs_2AgNaInCl_6$:Bi NCs solutions, two samples were considered changing slightly the different solvents mixtures and with different concentrations. We observed that ink concentration is the key parameter to ensure printability and consequently, a high uniformity of the printed layers.

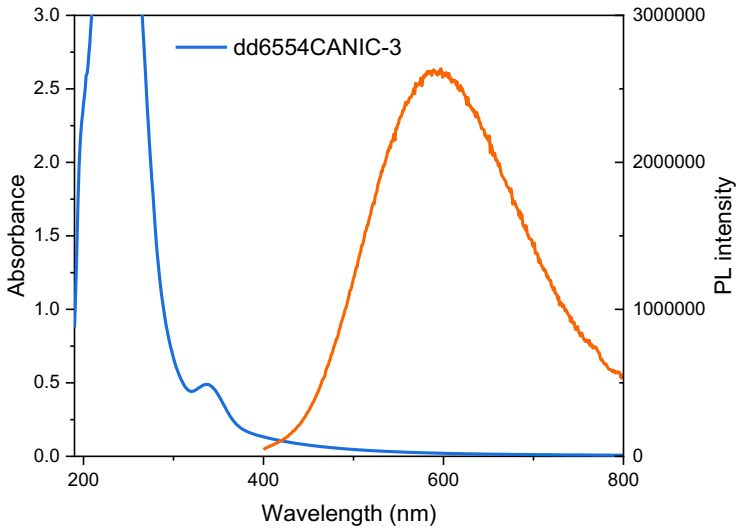

Figure 7. Optical properties of $Cs_2AgNaInCl_6$:Bi NCs films

In the following is presented a summary of all tested inks for emissive RGB devices along the project.

TABLE OF G-LFP MATERIALS/LAYERS

B-LFP	E_G (eV)	E_{PL} / I_{PL} (nm/eV)	LIFETIME/PLQY	SYNTHESIS	Spincoating	Inkjet printing	Device	CONTINUE
$MASnBr_3$ $(FA\text{-}MA)SnI_3$ $FASnBr_3$	2.5	600 550 500	LOW	precursors		Yes – to be Optimized	Try LED ¿?	NO

TABLE OF G-LFP MATERIALS/LAYERS

G-LFP6	E_G (eV)	I_{PL}/E_{PL} (nm/eV)	LIFETIME/PLQY	SYNTHESIS	Spincoating / other	Inkjet printing	CONTINUE Yes/No
Sn:CsBr Cs_4SnBr_6	2.92 3.68	610 / 2.05 550	- / 20 % - / 2 %	Direct precipitation - powder	Yes	Yes	NO
$Cs_2Ag_{0.4}Na_{0.6}InCl_6$:Bi	4.2/3.5	590 / 2.1	- / 12 %	Hot injection - NCs		Yes	TRY - LED
Rb_3InCl_6:Sb	> 3.65	505	- / 13 % - / 85 %	NCs precursors		Yes Yes	YES - LED
$Cs_3Cu_2I_5$ $Cs_3Cu_2Cl_5$ $CsCu_2Cl_3$	4.35 4.35 4.9	450 525 454	100 100 65	Hot injection NCs	Yes		YES - LED
$Cs_3Cu_2I_5$	>4.1	450	- / 85 %	precursors		Yes	YES - LED
$(OLAm)_2SnBr_4$	3.9	620	100	Hot injection NCs		Yes	NO
$(PEA)_2SnI_4$	2	630 nm			Yes	Yes	YES – LED SOLAR CELL LASER
TEA_2SnI_4	2.03	635-665	- / 23 %	precursors		Yes	YES – LED SOLAR CELL LASER

2.2 Inkjet printing conditions

All the materials were inkjet printed on flexible PI and PET/ITO/PEDOT:PSS substrates using Dimatix Materials Printer DMP-2850 equipment located and operated inside a glovebox in inert conditions. A scalable square pattern from 1 mm^2 up to 1 cm^2 is inkjet printed with different thicknesses to study the large-scale area reliability of printed thin films. The optimization of the printing process for each ink solution requires of two main steps:

1) Samples were inkjet printed with different drop spacing in the range of 20 µm to 50 µm to carry out the best value that promote the complete uniform thin layer without pinholes. The optimized drop spacing allow controlling the minimum thickness and obtaining the lowest roughness of the thin film. By printing several steps to reach the expected thickness the amount of solution of the layer is subsequently kept on the platen printer (pre-annealing) in the range of 30 °C to 60 °C.

2) After receiving a stable, dry layer with the expected colour for each material, samples were annealed at 110 °C for 10 minutes in a mini hot vacuum hotplate into the glovebox. The pre-annealing step is applied during the printing process to avoid local de-wetting of the precursor ink.

For the characterization of the printed thin layers we used also different substrates depending on the analysis to be performed, but basically silicon (PL measurement), fused silica (TRA measurements) and flexible substrates (morphology and structural inspections). The substrates were cleaned by ultrasonicator bath with detergent (Hellmax, 1ml over 100ml deionized water), acetone, deionized water and isopropanol for 20 minutes, respectively, and then treated with UV light for 10 minutes. Filtered solutions of perovskite nanocrystal ink were printed through 21-µm-nozzle by using a cartridge of Dimatix printers (Fujifilm Dimatix Inc.) on the cleaned substrate. The preparation of the inks was carried out in the glove box as the printing processes.

2.2.1 Devices

Only perovskite inks for red, green and blue emission, namely TEA_2SnI_4 (ETHZ) and PEA_2SnI_4 (UJI) for RED emission, $Rb_3InCl_6:Sb^{3+}$ for GREEN emission and $Cs_3Cu_2I_5$ for blue emission, have been received, printed and characterized at UB.

Once the active emissive layers have been characterized and validated via the inkjet printing method, a planning of device structures has been developed.

Fabrication of this structures would require additional studies of ink-layer compatibilities between the different layers, which already underway.

For some of the layers, additional methods to inkjet printing (such as spin coating or thermal evaporation) are also considered as quick solutions to possible problems that could appear, aiming for a fast fabrication of devices to quickly move to full inkjet-printed ones afterwards.

Taking into account the band alignments of validated transport layers in the previous deliverable D2.2 we fabricated several devices which have been tested in both configurations, *p-i-n* (standard) and *n-i-p* (inverse) structures respectively.

Below is presented a summary of the device fabrication. We produce each time two structures to validate the manufacturing processes. The first option is the validation of the inkjet-printed emissive layer, which means that the top transport layer and the top contact are evaporated by the partner

UJI into glovebox. The second option is the validation of the fully printed devices (p-i-n and n-i-p when possible) with only the metal top contact evaporated.

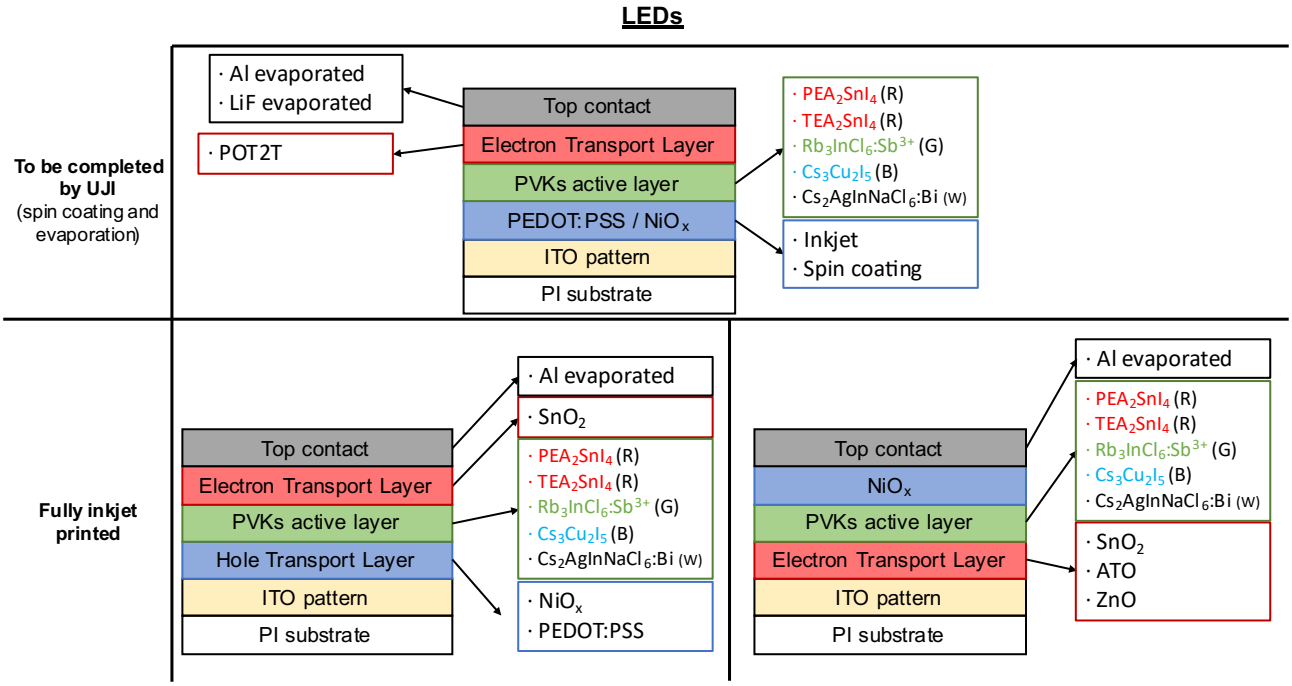

Figure 8. Planning of partial and fully inkjet-printed LEDs device into glovebox, inert conditions (N_2).

2.3 Material and preliminary device characterization

The morphology of the films obtained with all the inks was characterized via SEM and optical microscopies in order to observe the uniformity of the films and the effect of printing different amounts of layers and different curing processes. This allowed obtaining the best conditions for producing pin-hole free layers. These results were combined with XPS measurements that allow characterizing the composition of the layers and XRD to determine crystalline structure and micro/nanocrystal size. Finally, optical analysis like absorbance and PL (photoluminescence) spectra allows measuring band gap and confirm if the layers are optically active with the expected emission for each material.

To investigate the structural quality of the inkjet printed thin films XRD and SEM measurements were conducted, UV-vis spectroscopy allowed to probe the optical properties. MiniFlex Rigaku x-ray diffraction (XRD) instrument, Phenom ProX Desktop SEM from Phenom-World, FS5 Spectrofluorometer from Edinburgh Instruments Ltd, Bruker Dektak XTL Profilometer and Sun 3000 Class AAA form Abet Technologies were used.

3 Results

3.1 Structural, optical and morphological properties of the inkjet printed benchmark Sn^{2+}-based thin films for RED and YELLOW EMISSION.

3.1.1 $FASnBr_3$, $MASnBr_3$ from precursors (from SAULE)

The processing of the organic-inorganic tin halide perovskites $ASnBr_3$ (A=FA, MA) from molecular precursors (provided by the partner SAULE) showed good printability and stability in inert conditions as required. Figure 9 (on the left) shows the received solutions and their expected colours. After inkjet printing the two inks onto silicon and fused silica substrates, respectively, we can appreciate the predictable colours for each annealed samples: yellowish for the $FASnBr_3$, dark grey for the $FASnI_3$, reddish for the $MASnBr_3$ and light black for the $MASnI_3$ (Figure 9 on the right).

Figure 9. $FASnBr_3$, $MASnBr_3$ inkjet printed layers into glovebox, inert conditions (N_2). Ink bottles and optical photo with expected colors for each ink onto silicon and fused silica for PL (under laser of 488nm) and TRA measurements, respectively.

The vehicles of the inks (DMSO:DMF) allows for using a huge range of pre-annealing temperature, but we observed suddenly strong crystallization of printed layer for temperature over 30 ºC. All printing process were ensuring a homogeneous and compact layer when a drop space of 25 µm is employed. When the drop spacing is increased, in order to reduce the time of printing process, a not controlled patterning is promoted and no homogeneity in the thickness is observed. In conclusion, printing at room temperature as pre-annealing temperature results in more uniform thin films and promote a reduced crystallization significantly, while the best suitable drop spacing value is 25 µm, allowing to keep the final layer thickness for each layer in a controlled range.

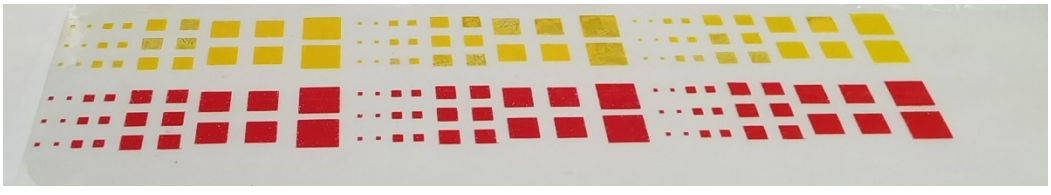

Figure 10. Inkjet printed layers from the top: $FASnBr_3$ (yellowish), $MASnBr_3$ (reddish).

After the pre-annealing temperature onto the printer platen, all the material has been annealed in a mini hot vacuum holder for hotplate (Figure 18) at 110ºC for 15 minutes.

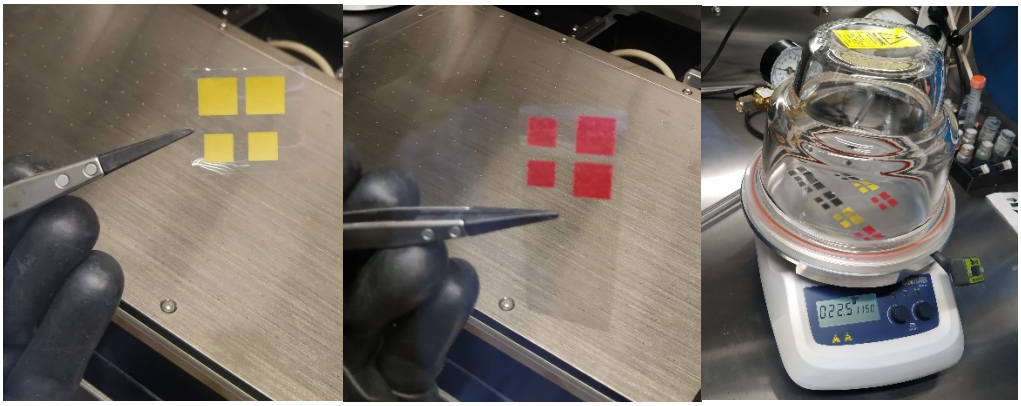

Figure 11. Detail of Inkjet printed layers (on the left) from the top: $FASnI_3$ (dark graphite), $MASnI_3$ (light graphite), $FASnBr_3$ (yellowish), $MASnBr_3$ (reddish). On the right side, a mini hot vacuum hotplate is employed for the annealing process.

The first characterization that allows us confirming the good quality of the layer is related to the absorbance curve from the transmittance, reflectance and absorbance (TRA) measurements (Figure 12) obtained in ambient conditions after passivating the sample with PMMA. All the samples clearly show a strong absorbance at the expected ranges demonstrating the uniformity of the layer.

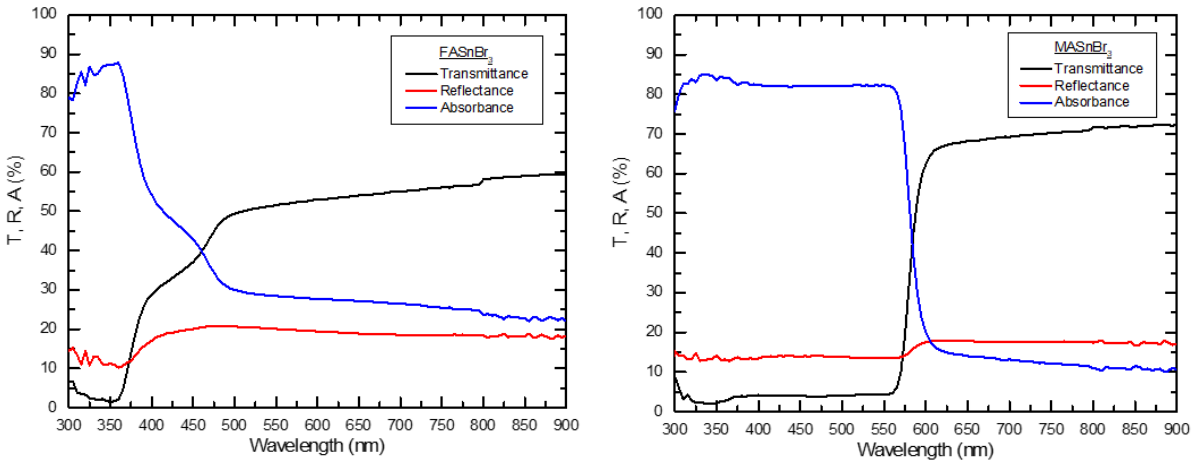

Figure 12: $FASnBr_3$, $MASnBr_3$ TRA measurements.

The consequent estimation of the bandgap of the materials is calculated from the Tauc plot with linear regression. Figure 13 shows from the Tauc plot the bandgap estimated for each inkjet printed layer, being very close to the expected one in literature.[3,4,7]

The printed layer based on $FASnI_3$ seems from the preliminary tests does not present a spectrum changing over time. The rest of the inkjet printed materials showed as fast degradation over the time. Still, we are studying the possible origin of this instability.

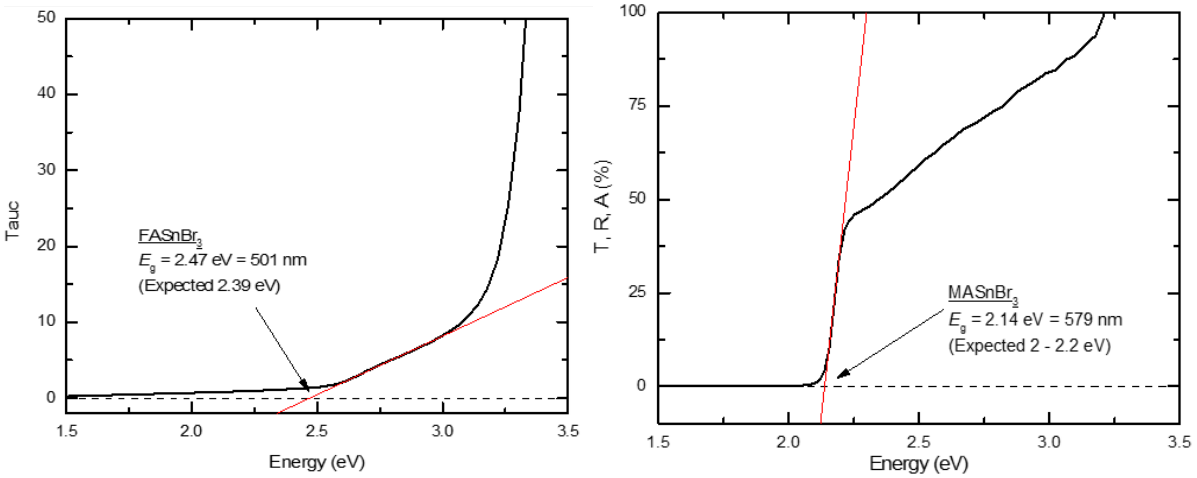

Figure 13: $FASnBr_3$, $MASnBr_3$ estimation of bandgaps from TRA measurements by Tauc plot linear regression.

The crystalline structure and orientation of the printed films were investigated by XRD, the results being shown in Figure 14. The XRD patterns clearly show the characteristic reflections of the expected cubic phases $Pm\bar{3}m$ space group at room temperature, as predicted from the nature of the nanocrystals.

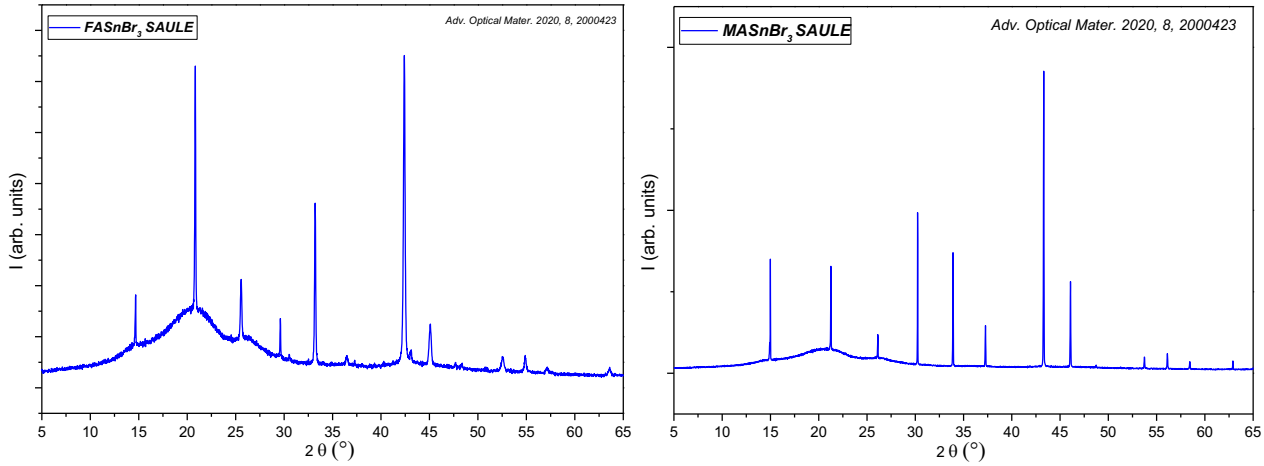

Figure 14: XRD pattern of $FASnBr_3$ and $MASnBr_3$ showing the main preferential crystallographic planes according to cubic phase in literature.

The surface uniformity on the microscopic scale showed no direct relationship with drop spacing or with pre-annealing temperature values.

Figure 15 shows a panel of SEM images of inkjet printed layers with very good resolution and large-scale uniformity and less homogeneity. No pinholes have been detected but some local instabilities appear at the surface of the layers. The thickness determined is similar to the one determined from the optical interferences although it is clear that there are large inhomogeneities.

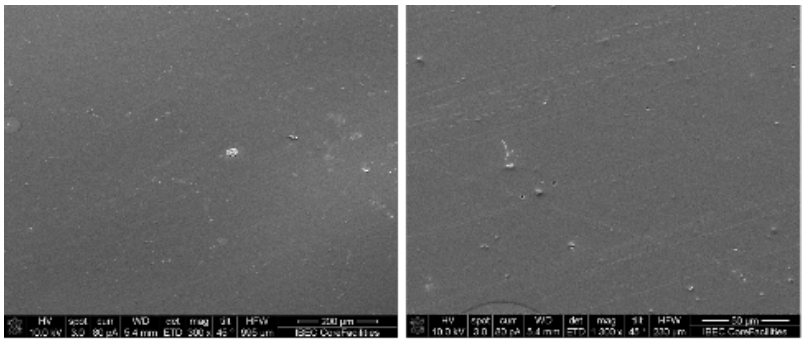

$FASnBr_3$

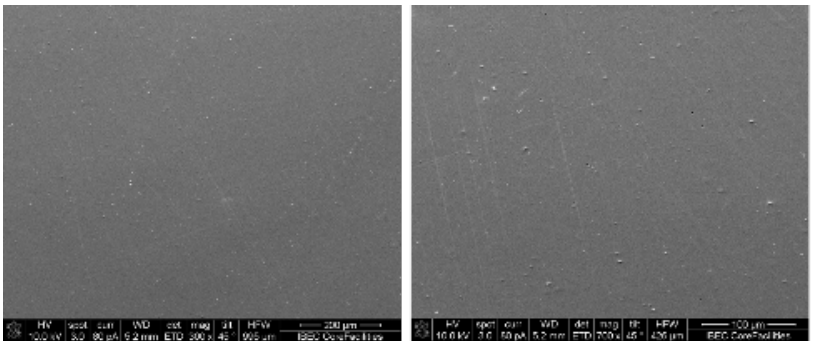

$MASnBr_3$

Figure 15: SEM images of $FASnBr_3$, $MASnBr_3$, on PI flexible substrate.

Finally, a qualitative inspection of inkjet-printed layers on top of flexible substrates has been carried out. To this end, the Sn^{+2}-based perovskite from molecular precursors have been inkjet-printed over most promising substrate PET and PI for the following study in other workpackages. Images were acquired by placing the substrate over a glass slide and illuminating from the top to obtain a better contrasted image.

The characterized layers were printed in a 8 × 8 mm^2 square shape. Figure 16 displays a panel of images for the different materials ($FASnI_3$, $MASnI_3$, $FASnBr_3$, $MASnBr_3$), for 4x and 10x objectives.

From these images it can be remarked, following the observations of SEM characterization, that printed layers are continuous and present a flat surface. Some macrostructures can be observed in all samples due to the expected crystallization of the precursors. Pinhole-free layers are obtained along the large-scale printing patterns from 1 mm^2 to 25 cm^2.

From these data we can conclude that the printed films are very uniform with polycrystalline structure. These optical measurements are aligned with the literature, but very low PL signal (PLQY well below 1% and poor stability) was observed (see Figure 17) due to fast degradation under laser excitations. We are still studying to stabilize the layers in order to be implemented for LEDs.

For the rest of materials in the following, images of the inkjet-printed films on flexible substrates and parts of their characterization process are presented divided into blue, green and white emissive layer.

Last but not least, for the RED emissive layers a deeper characterization of the inkjet printed LED devices will be displayed.

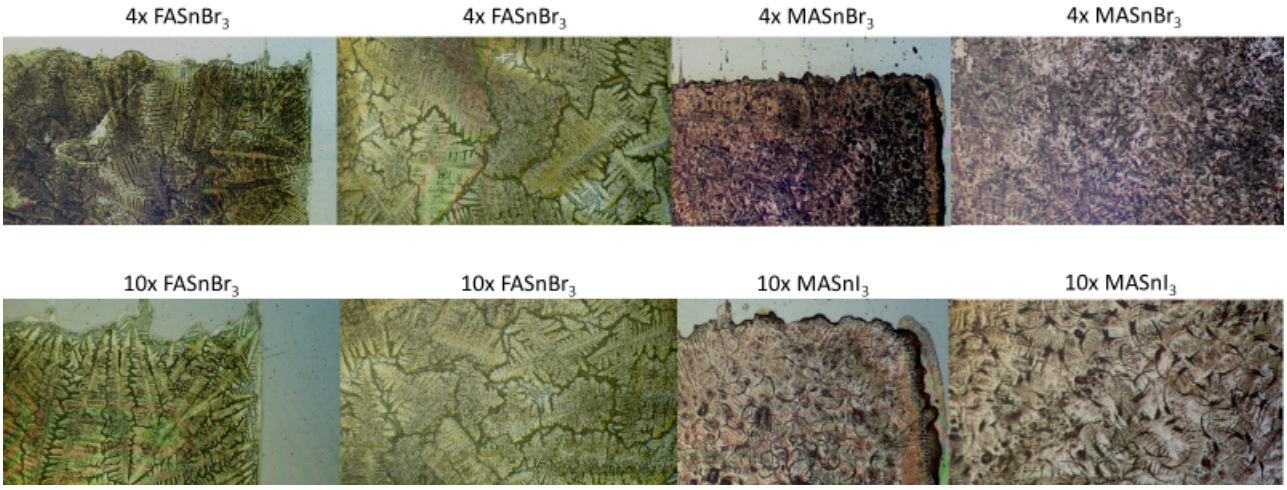

Figure 16: Optical images of $FASnBr_3$, $MASnBr_3$ on flexible substrate, area of 1.5 x 2.6 mm^2 for 4x magnification.

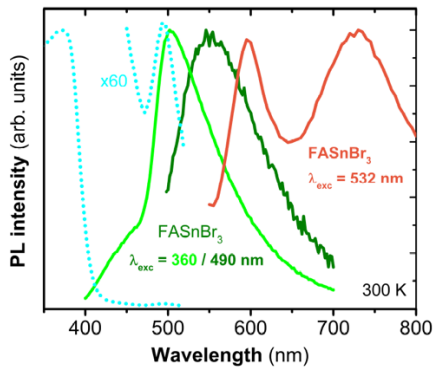

Figure 17: PL spectra of Inkjet printed films on PI of $FASnBr_3$ mesured under excitations at 360 and 490 nm (light and dark green curves) and $MASnBr_3$ under excitation at 532 nm (red curve), and PLE for the $FASnBr_3$ film (cyan dotted line).

3.2 Structural, optical and morphological properties of the inkjet printed $Cs_3Cu_2I_5$ pseudo-perovskites thin films for BLUE EMISSION

3.2.1 $Cs_3Cu_2I_5$ from precursor (from ETHZ)

Figures 18 – 23 show the ink containing the precursor of $Cs_3Cu_2I_5$ G-LFP (from ETHZ), inkjet printed films, together with morphological, structural and optical characterization (see the figure captions for the corresponding descriptions).

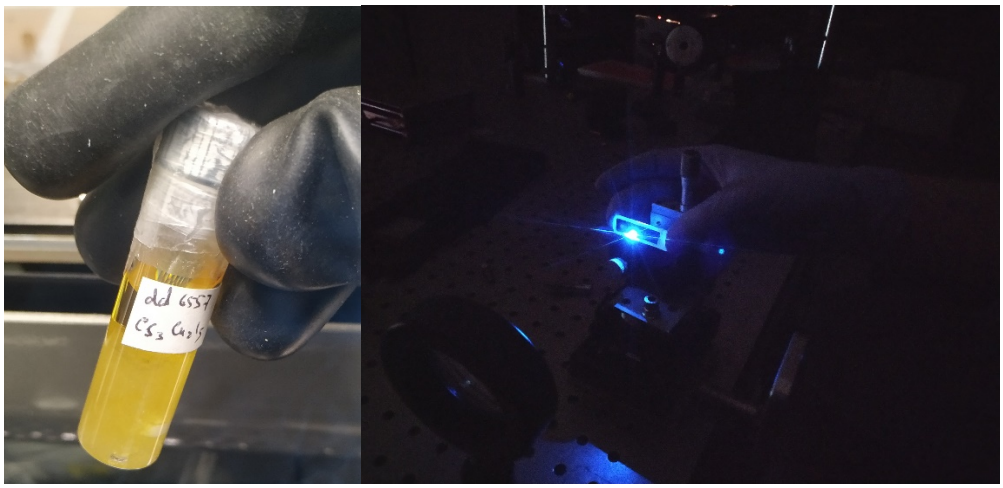

Figure 18: $Cs_3Cu_2I_5$ inkjet printed layers into glovebox, inert conditions (N_2). Ink bottle and PL colour under laser of 488nm.

Figure 19. Inkjet printed $Cs_3Cu_2I_5$ layer on PI flexible substrate. Pattern of squares ranging from 1 mm^2 to 1 cm^2.

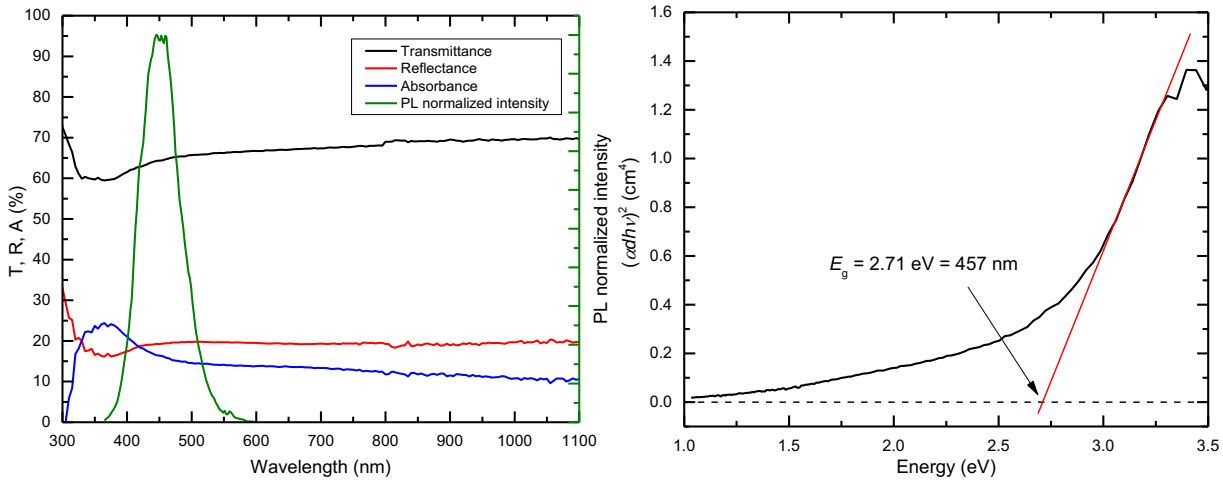

Figure 20: left) Combined measurements of TRA and PL of $Cs_3Cu_2I_5$ inkjet printed on silicon into glovebox, inert conditions (N_2). Expected PL signal with emission in the red colour. right) $Cs_3Cu_2I_5$ estimation of bandgaps from TRA measurements by Tauc plot linear regression.

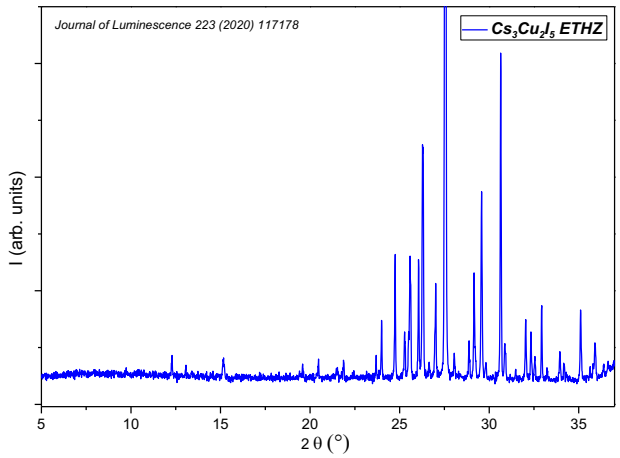

Figure 21: XRD pattern of $Cs_3Cu_2I_5$ showing the main preferential crystallographic planes according to tetragonal phase in literature.

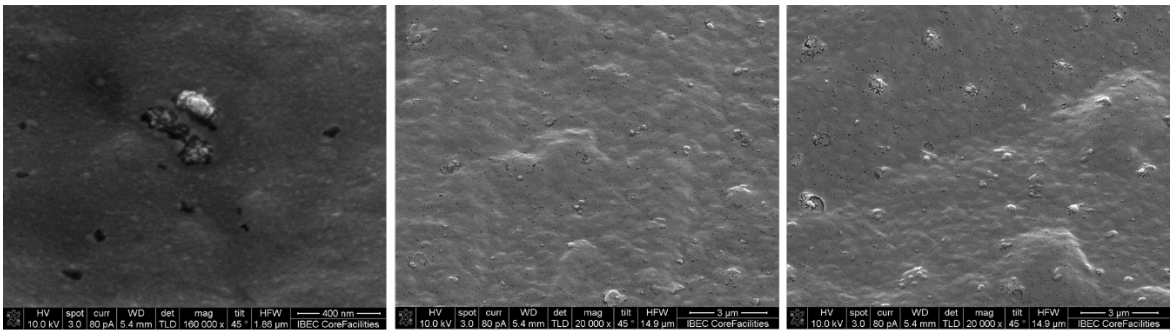

Figure 22: SEM images of $Cs_3Cu_2I_5$ on PI flexible substrate.

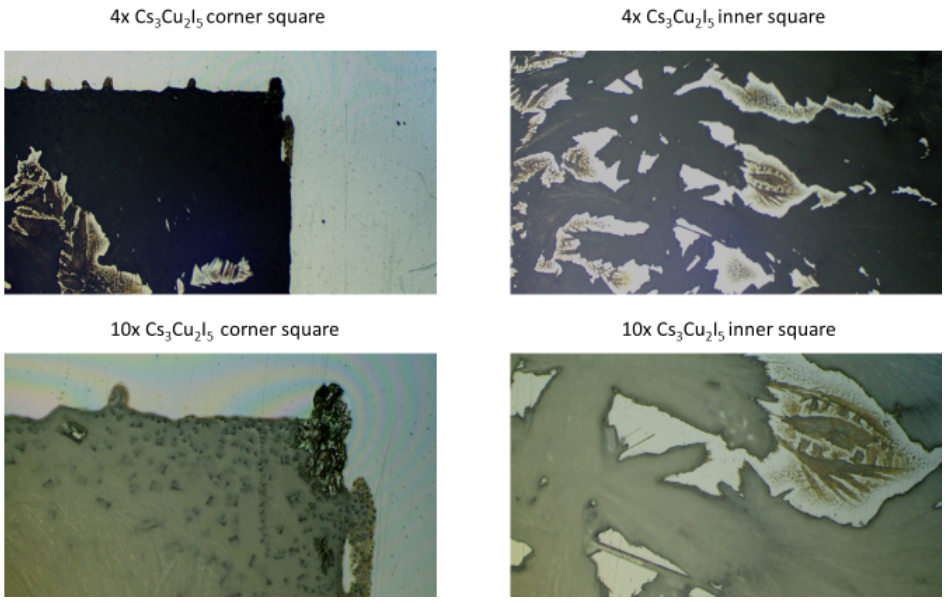

Figure 23: Optical images of $Cs_3Cu_2I_5$ on flexible substrate, area of 1.5 x 2.6 mm^2 for 4x magnification.

3.2.2 $Cs_3Cu_2I_5$ from NCs (from UJI)

Figures 24 – 28 show the ink containing the precursor of $Cs_3Cu_2I_5$ G-LFP (from UJI), inkjet printed films, together with morphological, structural and optical characterization (see the figure captions for the corresponding descriptions).

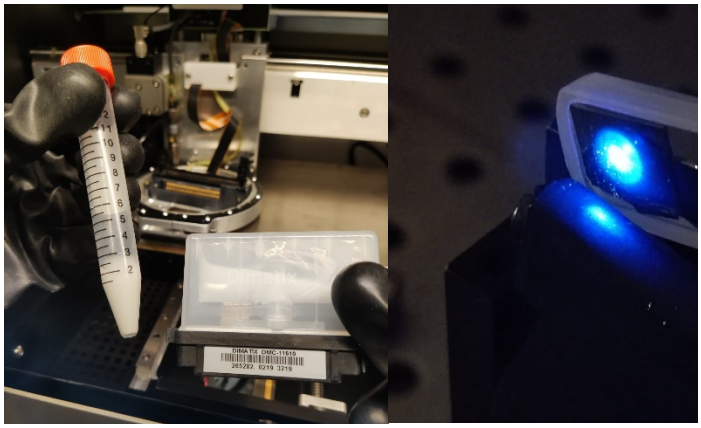

Figure 24: $Cs_3Cu_2I_5$ inkjet printed layers into glovebox, inert conditions (N_2). Ink bottle and PL colour under laser of 488nm.

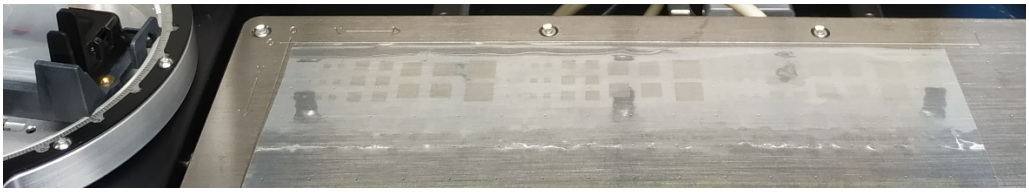

Figure 25: Inkjet printed $Cs_3Cu_2I_5$ layer on PI flexible substrate. Pattern of squares ranging from 1 mm^2 to 1 cm^2.

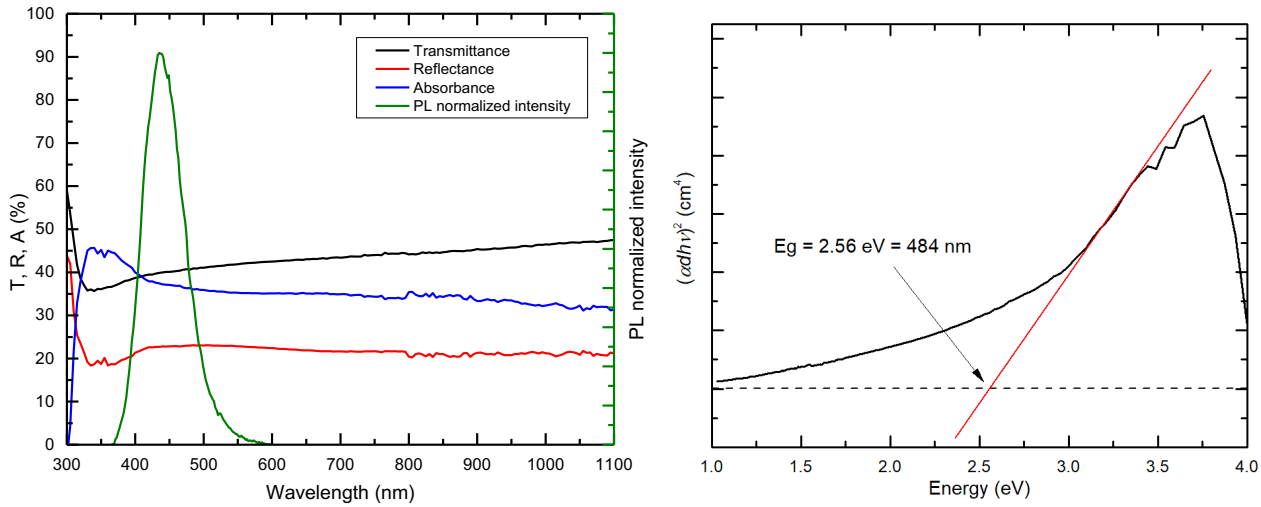

Figure 26: left) Combined measurements of TRA and PL of $Cs_3Cu_2I_5$ inkjet printed on silicon into glovebox, inert conditions (N_2). Expected PL signal with emission in the red colour. right) $Cs_3Cu_2I_5$ estimation of bandgaps from TRA measurements by Tauc plot linear regression.

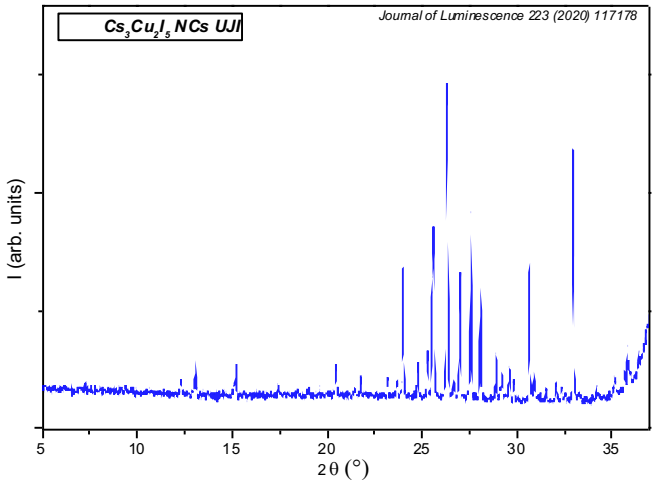

Figure 27: XRD pattern of $Cs_3Cu_2I_5$ showing the main preferential crystallographic planes according to tetragonal phase in literature.

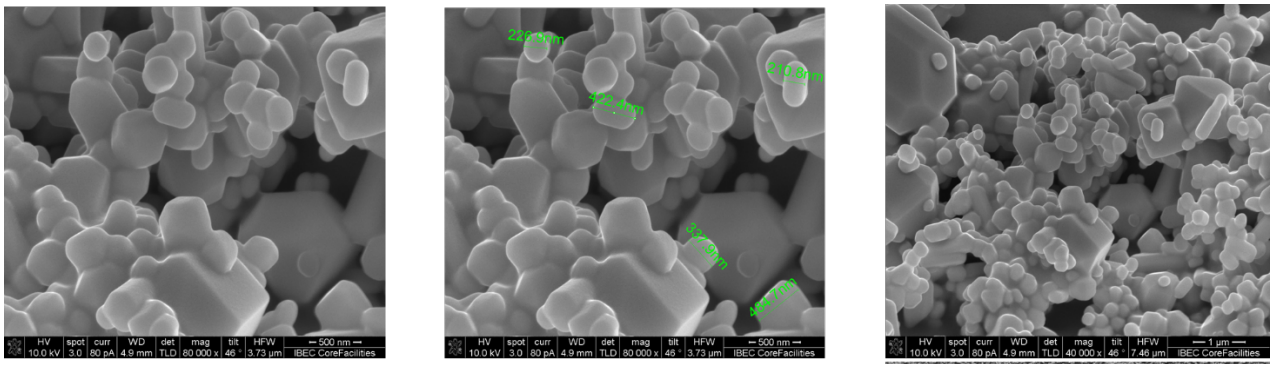

Figure 28: SEM images of $Cs_3Cu_2I_5$ on PI flexible substrate.

3.3 Structural, optical and morphological properties of the inkjet printed $Cs_2AgNaInCl_6:Bi^{3+}$ pseudo-perovskites thin films for WHITE EMISSION

3.3.1 $Cs_2AgNaInCl_6:Bi^{3+}$ from NCs (from ETHZ)

Figures 29 – 32 show the ink containing the precursor of $Cs_2AgNaInCl_6:Bi^{3+}$ G-LFP (nanocrystaals synthesized by ETHZ), inkjet printed films, together with morphological, structural and optical characterization (see the figure captions for the corresponding descriptions).

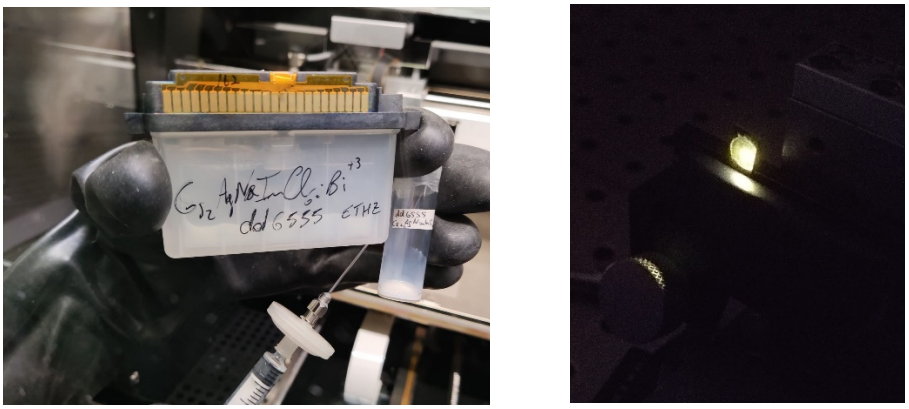

Figure 29: $Cs_2AgNaInCl_6:Bi^{3+}$ inkjet printed layers into glovebox, inert conditions (N_2). Ink bottle and PL colour under laser of 488nm.

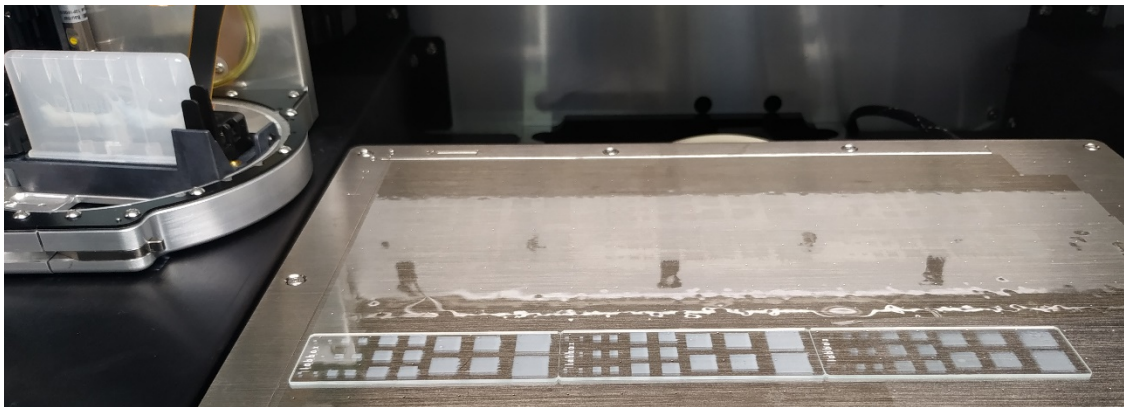

Figure 30: Inkjet printed $Cs_2AgNaInCl_6:Bi^{3+}$ layer on PI flexible substrate (transparent patterns) and glass slide. Pattern of squares ranging from 1 mm^2 to 1 cm^2.

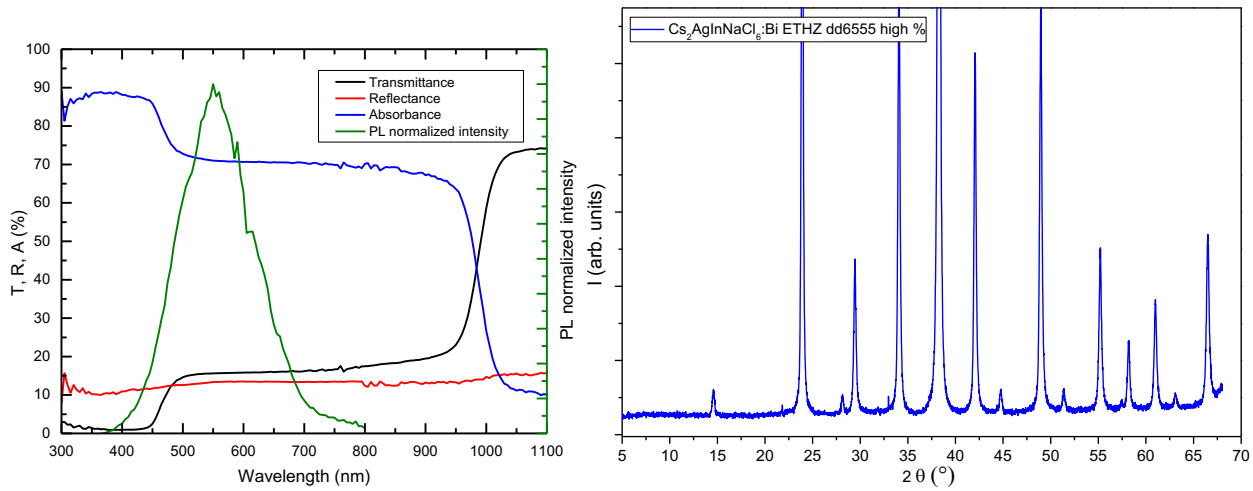

Figure 31: left) Combined measurements of TRA and PL of $Cs_2AgNaInCl_6:Bi^{3+}$ inkjet printed on silicon into glovebox, inert conditions (N_2). Expected PL signal with emission in the red colour. right) XRD pattern of $Cs_2AgNaInCl_6:Bi^{3+}$ showing the main preferential crystallographic planes according to tetragonal phase in literature.

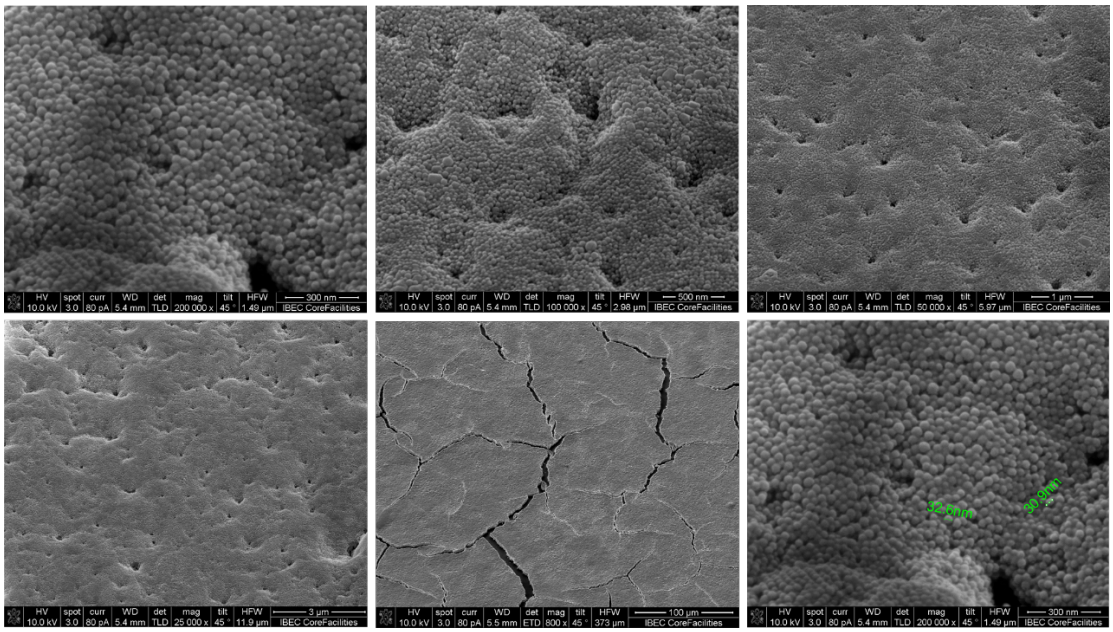

Figure 32: SEM images of $Cs_2AgNaInCl_6$:Bi^{3+} on PI flexible substrate.

3.4 Structural, optical and morphological properties of the inkjet printed 2D perovskites TEA_2SnI_4 and PEA_2SnI_4 thin films for RED EMISSION

3.4.1 TEA_2SnI_4 from precursor (ETHZ)

An ink solution of TEA_2SnI_4 based on molecular precursors dissolved on DMSO (Figure 33) has been prepared for inkjet printing technology. Successful fabrication of thin films of TEA_2SnI_4 (Figure 34) has been achieved by using this ink, modifying inkjet printing parameters and post-fabrication curing processes.

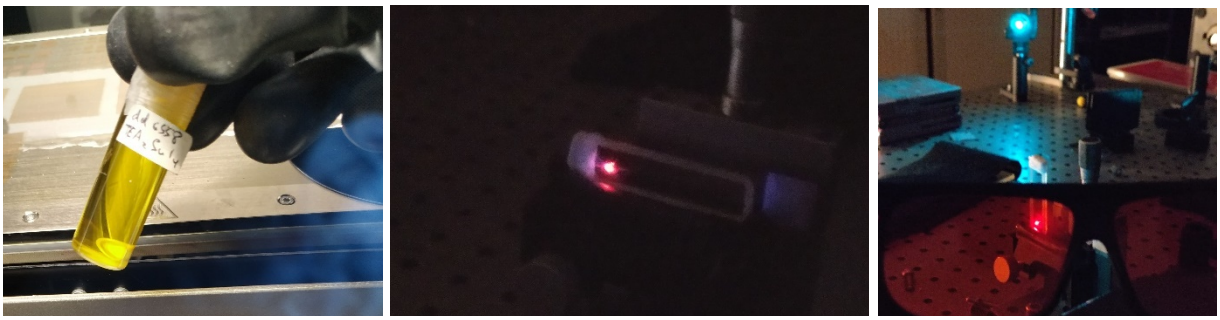

Figure 33. Ink bottle and PL colour under laser of 488nm of TEA_2SnI_4 inkjet printed layers into glovebox, inert conditions (N_2).

Figure 34. Inkjet printed TEA_2SnI_4 layer on PI flexible substrate emitting in the red range under UV pointer excitation. Pattern of squares ranging from 1 mm^2 to 1 cm^2.

Structural characterization performed by SEM and optical microscopy allowed determining the good uniformity of the films (uniform and pin-hole free) and monitoring the influence of printing different number of layers and curing processes on the final film features. XRD was employed to corroborate their tetragonal structure.

SEM images of inkjet printed layers on PI substrate with very good compactness, uniformity and homogeneity on the surface and low roughness (see Figure 35 – left). No pinholes have been detected. Optical microscope images of printed layers in an 8×8 mm^2 square shape. The panel of images displays the TEA_2SnI_4 for 4x and 10x objectives (Figure 35 – right). Printed layers are continuous and present a flat surface. Some macrostructures can be observed in all samples due to the expected crystallization of the precursors.

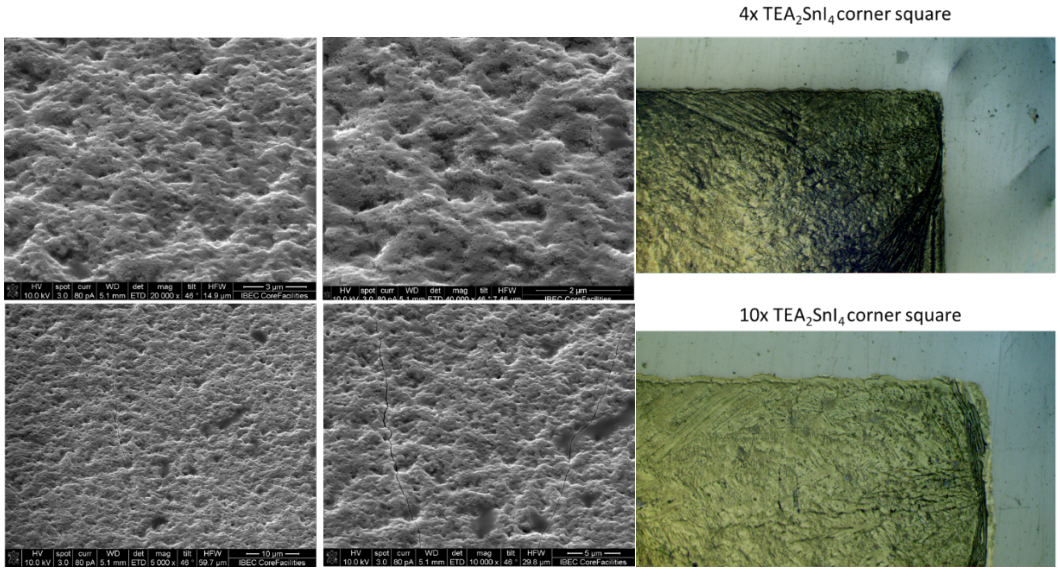

Figure 35: left) SEM images of TEA_2SnI_4 on PI flexible substrate; right) Optical images of TEA_2SnI_4 on flexible substrate, area of 1.5 x 2.6 mm^2 for 4x magnification.

The XRD pattern of TEA_2SnI_4 inkjet-printed films (Figure 36) from molecular precursors shows its main preferential crystallographic planes according to literature where a tetragonal phase is expected. [8]

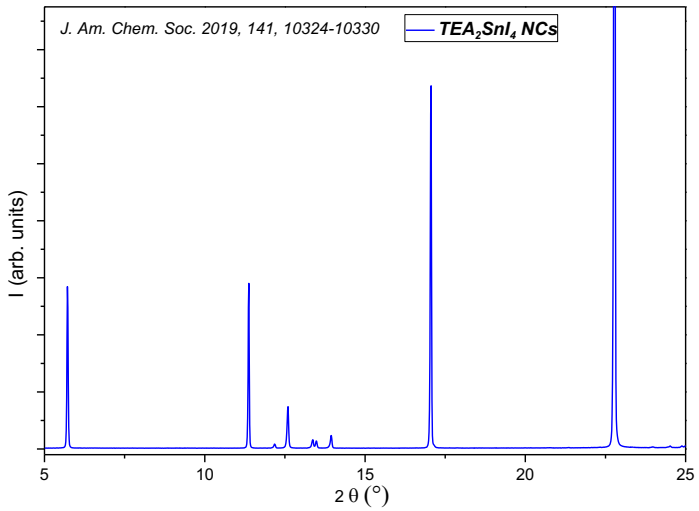

Figure 36: XRD pattern of TEA_2SnI_4 showing the main preferential crystallographic planes according to tetragonal phase in literature

Finally, the optical analysis through absorption and emission measurements revealed an optical band gap energy of 1.89 eV and a narrow emission at 1.95 eV, as observed in Figure 37. Good quality of the printed layer is evidenced through the absorbance curve from the TRA measurements obtained in ambient conditions. Absorbance curve shows absorption starting at ~655 nm. From the Tauc plot a bandgap of 1.89 eV for the printed layer. Intense PL emission can be seen at 650 nm.

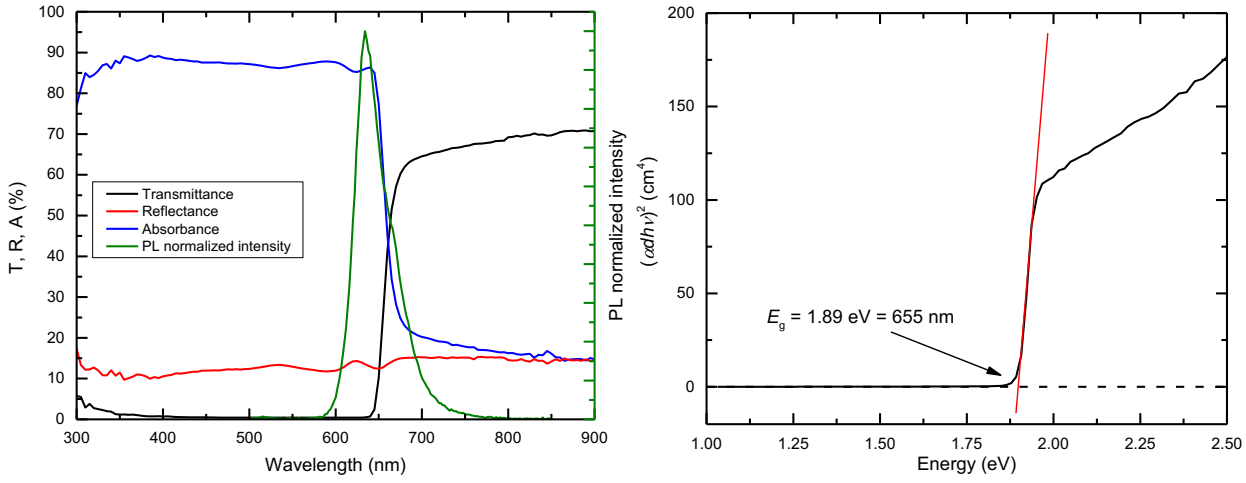

Figure 37. left) Combined measurements of TRA and PL of TEA_2SnI_4 inkjet printed on silicon into glovebox, inert conditions (N_2). Expected PL signal with emission in the red colour. right) TEA_2SnI_4 estimation of bandgaps from TRA measurements by Tauc plot linear regression.

Considering the band alignments of validated transport layers in the previous deliverable 2.2 we fabricated several devices which have been tested in both configurations, *p-i-n* (standard) and *n-i-p* (inverse) structures respectively.

The selected structure is ITO/PEDOT:PSS (spin-coated)/NiOx/TEA_2SnI_4/SnO_2/Ag(evaporated) and, as illustrated in Figure 38.

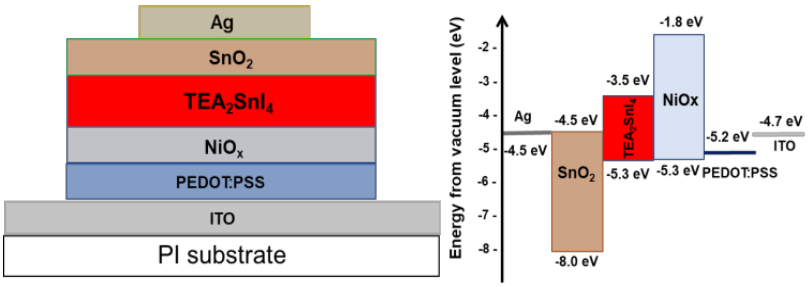

Figure 38. LED device with *p-i-n* structure and related band diagram chart.

The three first images in Figure 39 correspond to different steps in the fabrication. As a quick test of the stability of the emitting layer, a laser pointer is employed to observe that PL emission is maintained after each step. The *I*(*V*) curves of the devices are being performed inside the glovebox using a small measuring kit (last panel of the Figure). The devices did not exhibit short-circuits, but a negligible electroluminescence (EL) was observed. The work in this task will continue with new ink-batches of TEA_2SnI_4. We consider that the high concentration of the solutions received is promoting non-radiative recombination which reduces the possible electroluminescence.

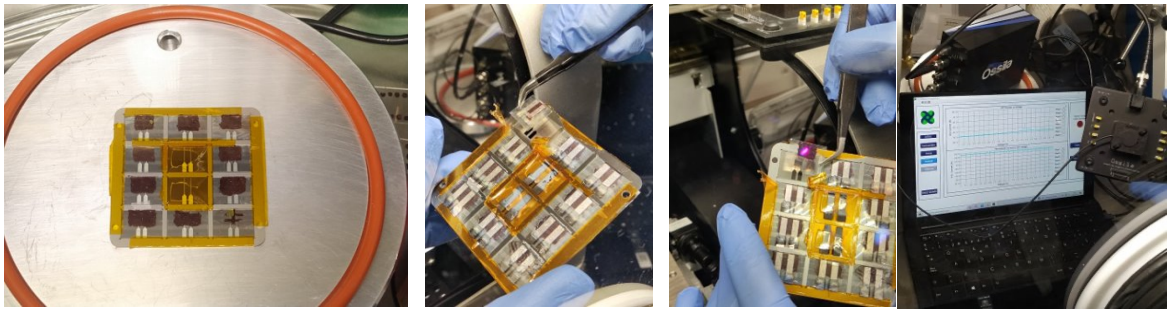

Figure 39. Fabrication of 10 inkjet-printed LEDs. **From left to right:** Visual inspection reveals TEA_2SnI_4 layers are uniform after hotplate curing of SnO_2 transparent layers printed on top; extraction of devices from the holder used for fabrication after evaporation of Ag contacts; PL emission in red using a 405 nm laser pointer confirms the perovskite layer is optically active in the finalized structure.

3.4.2 PEA_2SnI_4 from precursor (UJI)

Due to the lack of raw materials, the partner ETHZ was not able to provide a second batch of the TEA_2SnI_4 precursor with the same promising characteristics, as previously showed, until end of May 2022. Therefore, we focused on the preparation of LEDs by inkjet printing with single layers of the 2D PEA_2SnI_4 perovskite developed from a precursor solution from UJI team with the experience acquired during the collaboration among all the partners.

Thin layers have been prepared by inkjet printing technology using different additive into the PEA_2SnI_4 solutions, SnF_2 and SnF_2 + $NabH_4$, respectively. The devices developed here have the structure of ITO / PEDOT:PSS / NiO_x / PEA_2SnI_4 / POT2T / LiF : Al as presented in the following Figure 40.

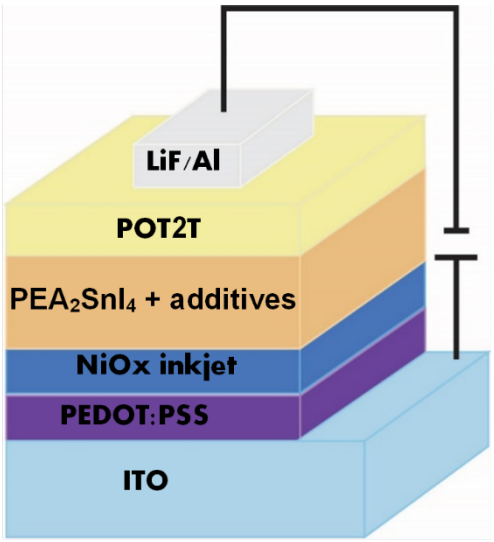

Figure 40. Device structure of inkjet printed PEA_2SnI_4-based LEDs

Due to the orthogonality property required to ensure maintaining the optical characteristic of the emissive printed layer, only the *p-i-n* structure for the moment was the working LED architecture. Figure 41 shows on the right the use of UV pointer to corroborate the PL emission after full device manufacturing.

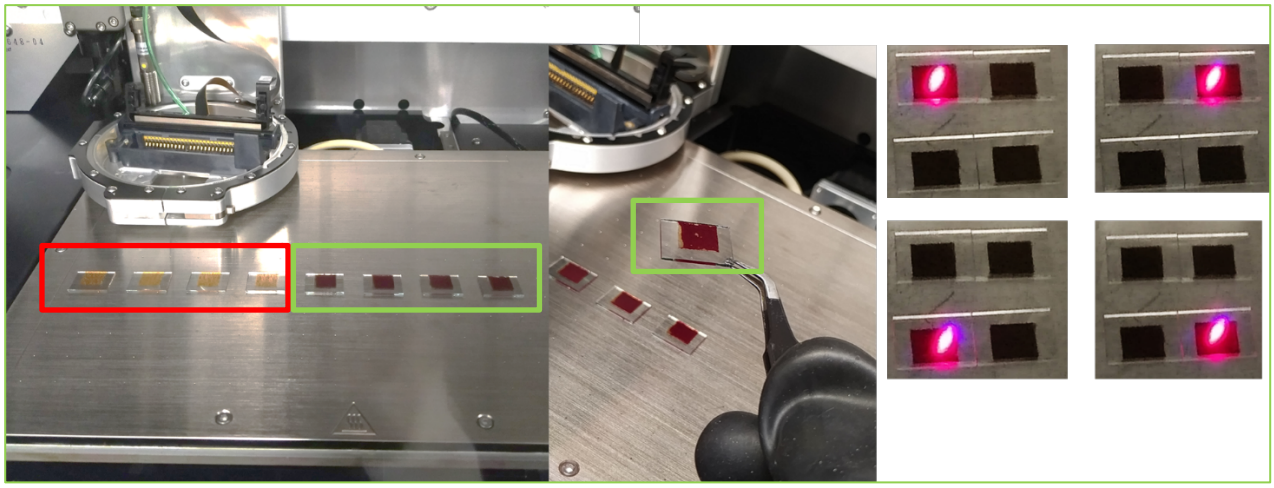

Figure 41. Device structure *n-i-p* (no orthogonality among inks) and *p-i-n* (very good orthogonality compatibility among inks) of inkjet printed PEA_2SnI_4-based LEDs. On the right UV pointer is employed to corroborate the PL emission after full device manufacturing.

Two main different inks of perovskite PEA_2SnI_4, with additives SnF_2 and $NaBH_4$, have been tested and showed the expected characteristic red EL. The fabricated devices are tested by portable SMU system of OSSILA which allows characterizing the LEDs both into and outside the glovebox environment (Figure 42 is a capture from the video **available in our Youtube DROP-IT channel**).

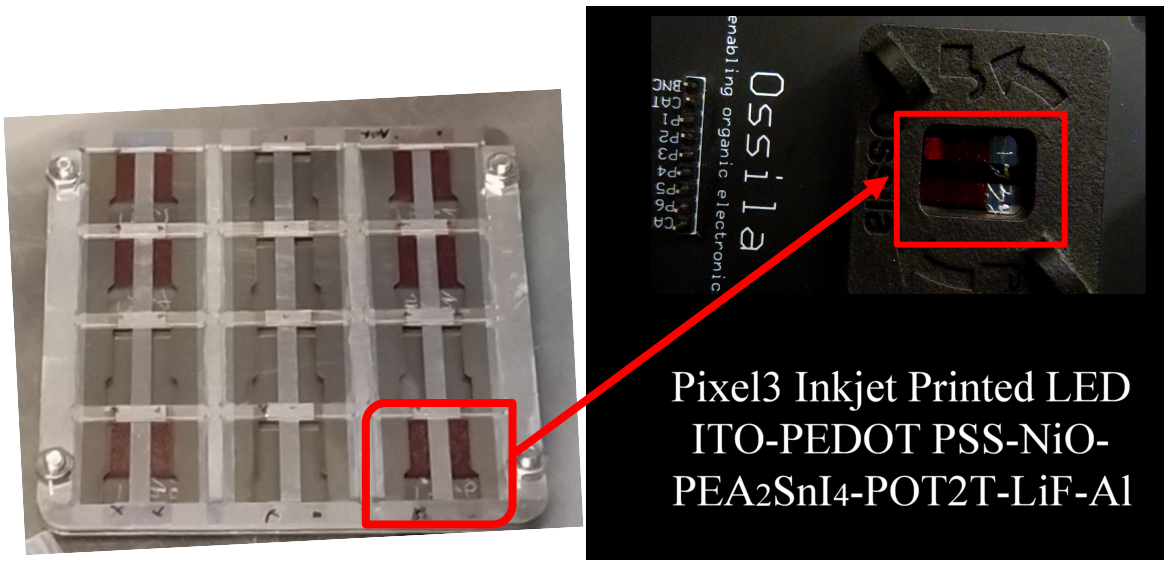

Figure 42. On the left the detail of printed LEDs devices on the mask substrate for the final metallic top contact. On the right the capture of a frame of the video (public in our Youtube DROP-IT channel).

The first devices presented the expected exponential I-V curve characteristic of LEDs devices, with current density around 2 mA/cm^2 and turn-on voltages of 4.5 V. These values were very promising, but the devices starts decreasing the current density and consequently also the EL after few iterations, as can be observed from Figure 43 (left).

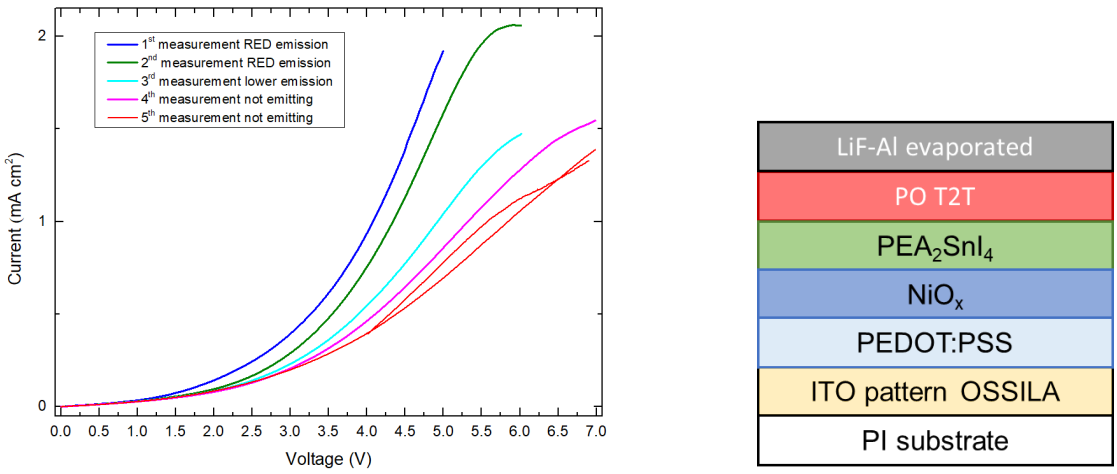

Figure 43. On the left the Current Density versus driving Voltage of printed LEDs devices. On the right the scheme of the tested LEDs devices.

The change of printing parameters, the use of only PEDOT:PSS as HTL (see scheme in Figure 43 – right) and the implementation of an improved protocol for the vacuum annealing process inside the glovebox allowed manufacturing new devices with improved performances in terms of stability and absolute values of EQE.

Figure 44. shows on the top the detail of printed LEDs devices and their emission under the applied voltage with common power supply (using alligator connectors into the glovebox) or by using automatic SMU system which allows lifetime measurements into and outside glovebox and analysing all the 6 LEDs for each substrate at the same time.

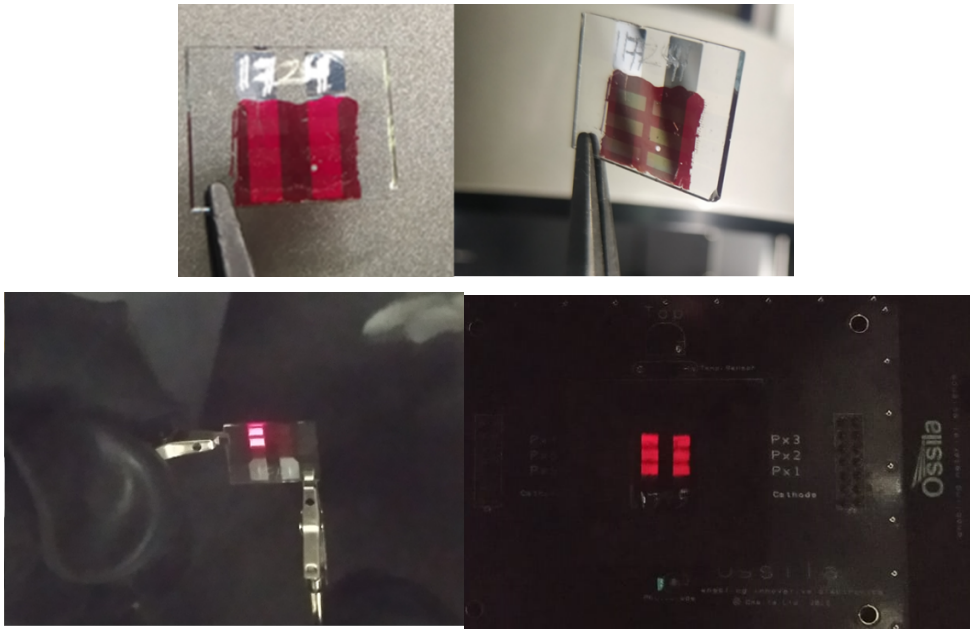

Figure 44: On the top the detail of printed LED devices. On the bottom the red emitting tested LEDs devices.

As can be observed in Figure 45, the current density increased and the lifetime test proved the stability of the devices with a slight drift, which corresponds to the same time with a lower EL.

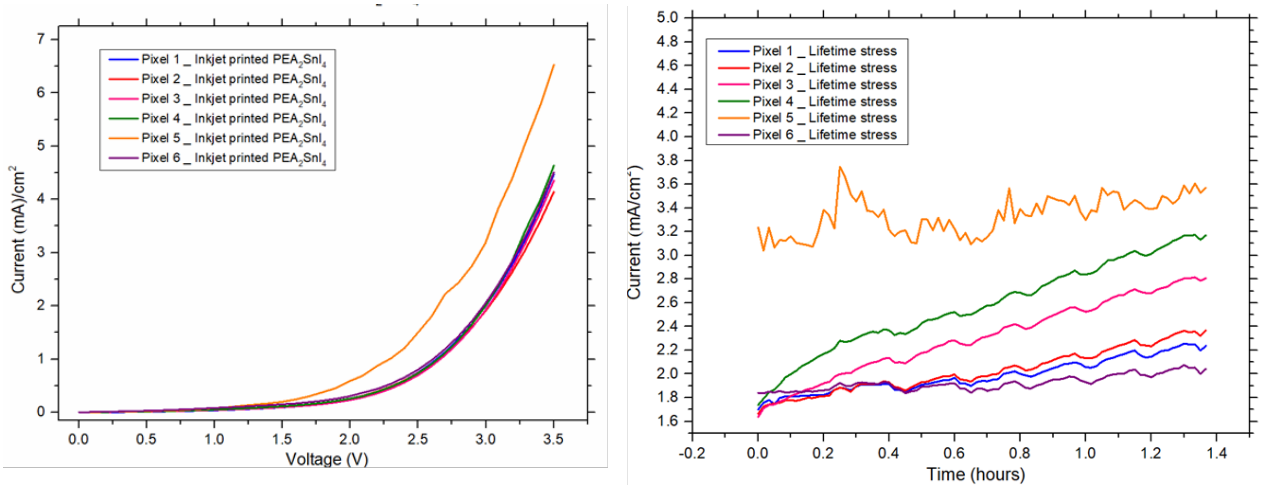

Figure 45: I-V and I-time curves of printed LED devices.

All the tested devices into glovebox are also analysed in ambient conditions after encapsulation (see pictures in Figure 46). The use of a UV paste promotes the printed layers degradation preserving only the active pixels.

Small degradation of the LEDs is observed in terms of turn-on voltages, probably due to the exposure of the LED devices to the UV lamp for the UV paste curing.

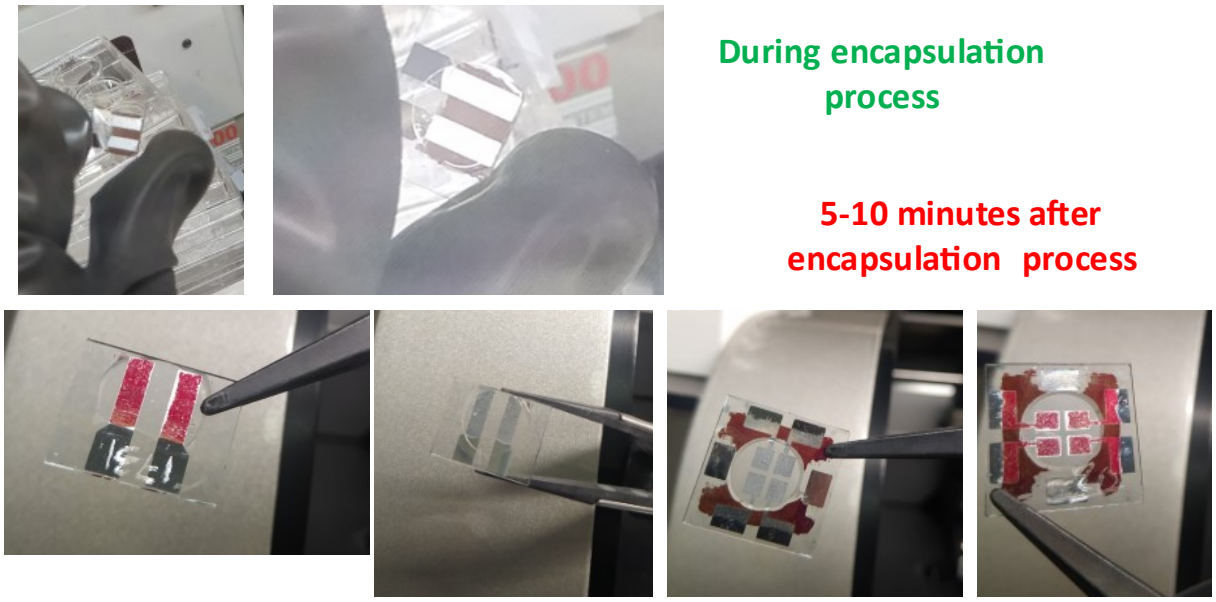

Figure 46: Encapsulation process of fabricated LEDs.

Figure 47 presents the comparison between the two possible inks solutions tested with different additives employed to reduce the oxidation of Sn^{2+} to Sn^{4+}. The number of layers corresponds to the emissive inkjet-printed layers with specific printing conditions.

Both solutions show very similar behaviour in terms of optoelectronics properties. The rheology of the inks is very different and determine a better (in case of only $NaBH_4$ as an additive) or worst (in case of both additives SnF_2 + $NaBH_4$) control of printed thickness.

The inkjet-printed PEA_2SnI_4-based LEDs exhibits a maximum external quantum efficiency (EQE) of 1% with an average of 0.7% (see Figure 48) and a brightness of 30 cd m^{-2} (Figure 48 – bottom), which are comparable to that of the control devices obtained by spin coating. Moreover, lifetime test shows an operating half-life exceeding 3 hours at an initial brightness of 10 cd/m^2.

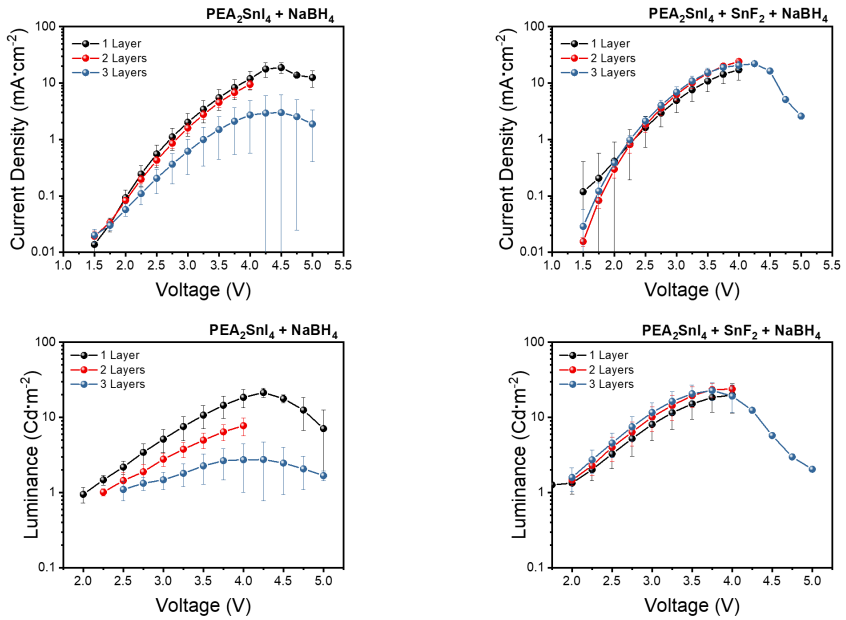

Figure 47: On the top the current density vs the driving voltage; on the bottom the brightness of the LED vs the driving voltage.

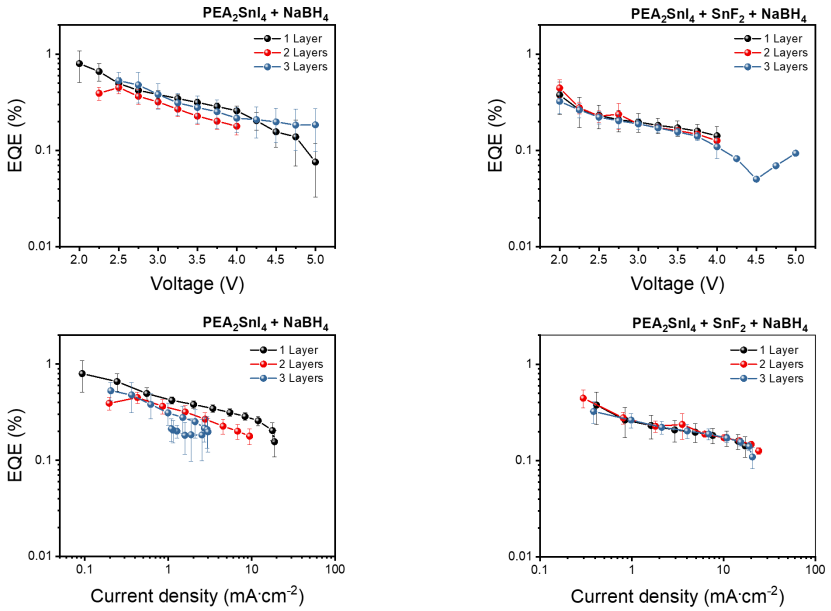

Figure 48: On the top the EQR vs the driving voltage; on the bottom the EQE of the LED vs the current density.

This work paves the way for inkjet-printed Cd- and Pb-free perovskite light-emitting devices for a wide variety of low-cost and customizable applications and will be the base of further developments and improvements for next deliverable centred on G-LFPs.

4 Deviations from the workplan

In these studies, not only inert conditions were investigated, but also feasibility in atmospheric conditions of LEDs devices. Ambient condition took more efforts due to the difficulties to develop the proper ink solution with the most appropriate additives with the best characteristics to be employed for printing process and annealing post process in combination with the suitable transport layers. Given the very low PLQY of $ASnBr_3$ (A=FA, MA, FA-MA) layers as B-LFPs for LEDs, which were prepared by inkjet printing using appropriate inks under inert atmosphere, the efforts were extended to novel LFPs (G-LFPs). Therefore, the research summarized here is still not completed at the moment, because it is the objective of the twin deliverable of this one. We have also included the preliminary investigations of red LEDs based on 2D tin perovskites as the most promising G-LFPs for this color. Similarly, the research also continues for developing green and blue emitting LEDs with high EQE, for which we have selected several promising G-LFPs.

5 Conclusions & Future directions

In this work, we demonstrated the formulation and printability of several RGB emissive B-LFP and new G-LFP materials by using inkjet printing technology to obtain highly emitting thin films with outstanding optical performance, large area, high reliability, and low-cost manufacturing. $ASnBr_3$ (A=FA, MA, FA-MA) inkjet-printed layers as B-LFPs were not demonstrated sufficiently high PLQY for LEDs and hence we concentrated the work to find alternative G-LFP materials for developing future red-green-blue LEDs, i.e., the main purpose of next twin deliverable of the present one, D4.4.

We successfully inkjet-printed red emitting LEDs based on 2D PEA_2SnI_4 perovskite as one of the most promising G-LFPs for LEDs, demonstrating the feasibility of the technology and the transfer & scalability from spin coating to inkjet printing techniques. The well-known degradation and instability issues were solved by selecting the most suitable additives (SnF_2 and $NaBH_4$) maintaining the best rheology of the inks and promoting the fast crystallization during the post process annealing in vacuum oven. Among all the tested devices, the inkjet-printed PEA_2SnI_4-based light-emitting diode (LED) is the one which exhibits, in ambient conditions after encapsulation, a maximum external quantum efficiency (EQE) of 1% with an average of 0.7% and a brightness of 30 cd m^{-2}, which are comparable to that of the control devices obtained by spin coating and the first in literature fabricated by inkjet printing. Moreover, lifetime test shows an operating half-life exceeding 3 hours at an initial brightness of 10 cd/m^2.

Future work (to be included in deliverable D4.4)

PEA_2SnI_4

- Reproducing all the emitting devices on all the available flexible substrates: PET, PEN, PI. We already have on PI substrate.
- Standardize the measurements protocol to ensure same value among the different partners.
- Encapsulation test with several polymers we used in the past for other applications.
- Improvement of the printing devices by using PEDOT:PSS doped with several options.
- Improving the stability by possible additives into the ink solution.
- Bending test of the devices.

TEA_2SnI_4

- Improving the ink printability from the several options proposed by the partner ETHZ carrying out the printing parameters to standardize the recipe.
- Reproducing all the emitting devices obtained with PEA_2SnI_4.
- Trying on flexible substrates: PET, PEN, PI. We already have on PI substrate.
- Demonstrating the higher quality of this 2D layered material by the optoelectronic measurements.
- Sending inkjet printed samples onto PI to partner UVEG to replicate the ASE observed in the past for this material.

$Cs_3Cu_2I_5$ and $Rb_3InCl_6:Sb^{3+}$

- We Improved the ink printability carrying out the printing parameters.
- Reproducing the best structure devices as the ones obtained with PEA_2SnI_4.
- Trying on flexible substrates: PET, PEN, PI.
- Finding possible solution to self-trapped excitonic emission in the 0D perovskite layered material.

Bibliography

(1) Majher, J. D.; Gray, M. B.; Liu, T.; Holzapfel, N. P.; Woodward, P. M. Rb3InCl6: A Monoclinic Double Perovskite Derivative with Bright Sb3+-Activated Photoluminescence. *Inorg. Chem.* **2020**, *59* (19). https://doi.org/10.1021/acs.inorgchem.0c02248.

(2) Han, P.; Luo, C.; Yang, S.; Yang, Y.; Deng, W.; Han, K. All-Inorganic Lead-Free 0D Perovskites by a Doping Strategy to Achieve a PLQY Boost from <2 % to 90 %. *Angew. Chemie - Int. Ed.* **2020**, *59* (31). https://doi.org/10.1002/anie.202003234.

(3) Ferrara, C.; Patrini, M.; Pisanu, A.; Quadrelli, P.; Milanese, C.; Tealdi, C.; Malavasi, L. Wide Band-Gap Tuning in Sn-Based Hybrid Perovskites through Cation Replacement: The FA1-:XMAxSnBr3 Mixed System. *J. Mater. Chem. A* **2017**, *5* (19). https://doi.org/10.1039/c7ta01668a.

(4) El Ajjouri, Y.; Igual-Muñoz, A. M.; Sessolo, M.; Palazon, F.; Bolink, H. J. Tunable Wide-Bandgap Monohalide Perovskites. *Adv. Opt. Mater.* **2020**, *8* (17). https://doi.org/10.1002/adom.202000423.

(5) Jiang, X.; Wang, F.; Wei, Q.; Li, H.; Shang, Y.; Zhou, W.; Wang, C.; Cheng, P.; Chen, Q.; Chen, L.; Ning, Z. Ultra-High Open-Circuit Voltage of Tin Perovskite Solar Cells via an Electron Transporting Layer Design. *Nat. Commun.* **2020**, *11* (1). https://doi.org/10.1038/s41467-020-15078-2.

(6) Mathies, F.; List-Kratochvil, E. J. W.; Unger, E. L. Advances in Inkjet-Printed Metal Halide Perovskite Photovoltaic and Optoelectronic Devices. *Energy Technol.* **2020**, *8* (4). https://doi.org/10.1002/ente.201900991.

(7) Mathies, F.; Eggers, H.; Richards, B. S.; Hernandez-Sosa, G.; Lemmer, U.; Paetzold, U. W. Inkjet-Printed Triple Cation Perovskite Solar Cells. *ACS Appl. Energy Mater.* **2018**, *1* (5), 1834–1839. https://doi.org/10.1021/acsaem.8b00222.

(8) Lin, J. T.; Liao, C. C.; Hsu, C. S.; Chen, D. G.; Chen, H. M.; Tsai, M. K.; Chou, P. T.; Chiu, C. W. Harnessing Dielectric Confinement on Tin Perovskites to Achieve Emission Quantum Yield up to 21%. *J. Am. Chem. Soc.* **2019**, *141* (26). https://doi.org/10.1021/jacs.9b03148.

(9) Lin, J. T.; Hu, Y. K.; Hou, C. H.; Liao, C. C.; Chuang, W. T.; Chiu, C. W.; Tsai, M. K.; Shyue, J. J.; Chou, P. T. Superior Stability and Emission Quantum Yield (23% ± 3%) of Single-Layer 2D Tin Perovskite TEA2SnI4 via Thiocyanate Passivation. *Small* **2020**, *16* (19). https://doi.org/10.1002/smll.202000903.

(10) Zhang, X.; Wang, C.; Zhang, Y.; Zhang, X.; Wang, S.; Lu, M.; Cui, H.; Kershaw, S. V.; Yu, W. W.; Rogach, A. L. Bright Orange Electroluminescence from Lead-Free Two-Dimensional Perovskites. *ACS Energy Lett.* **2019**, *4* (1). https://doi.org/10.1021/acsenergylett.8b02239.

(11) Das Adhikari, S.; Masi, S.; Echeverría-Arrondo, C.; Miralles-Comins, S.; Sánchez, R. S.; Fernandes, J. A.; Chirvony, V.; Martínez-Pastor, J. P.; Sans, V.; Mora-Seró, I. Continuous-Flow Synthesis of Orange Emitting Sn(II)-Doped CsBr Materials. *Adv. Opt. Mater.* **2021**, *9* (21). https://doi.org/10.1002/adom.202101024.

(12) Wang, L.; Shi, Z.; Ma, Z.; Yang, D.; Zhang, F.; Ji, X.; Wang, M.; Chen, X.; Na, G.; Chen, S.; Wu, D.; Zhang, Y.; Li, X.; Zhang, L.; Shan, C. Colloidal Synthesis of Ternary Copper Halide Nanocrystals for High-Efficiency Deep-Blue Light-Emitting Diodes with a Half-Lifetime above 100 H. *Nano Lett.* **2020**, *20* (5). https://doi.org/10.1021/acs.nanolett.0c00513.